This is a previous version of the article published in Applied Catalysis A: General. 2020, 593: 117442. doi:10.1016/j.apcata.2020.117442

CO_2 valorisation via Reverse Water-Gas Shift reaction using promoted Fe/CeO_2-Al_2O_3 catalysts: showcasing the potential of advanced catalysts to explore new processes design

L.Yang[1], L.Pastor-Pérez*[1,2], J.J.Villora-Pico[2], S.Gu[1], A.Sepúlveda-Escribano[2], T.R.Reina[1]

[1]*Chemical and Process Engineering Department, University of Surrey, Guildford, UK*

[2]*Laboratorio de Materiales Avanzados, Departamento de Química Inorgánica - Instituto Universitario de Materiales de Alicante Universidad de Alicante, Apartado 99, E-03080 Alicante, Spain.*

* corresponding authors: l.pastorperez@surrey.ac.uk

Abstract

The RWGS reaction represents a direct approach for gas-phase CO_2 upgrading. This work showcases the efficiency of Fe/CeO_2-Al_2O_3 catalysts for this process, and the effect of selected transition metal promoters such as Cu, Ni and Mo. Our results demonstrated that both Ni and Cu remarkably improved the performance of the monometallic Fe-catalyst. The competition Reverse Water-Gas Shift (RWGS) reaction/CO_2 methanation reaction was evident particularly for the Ni-catalyst, which displayed high selectivity to methane in the low-temperature range. Among the studied catalysts the Cu promoted sample represented the best choice, exhibiting the best activity/selectivity balance. In addition, the Cu-doped catalyst was very stable for long-term runs – an essential requisite for its implementation in flue gas upgrading units. This material can effectively catalyse the RWGS reaction at medium-low temperatures, providing the possibility to couple the RWGS reactor with a syngas conversion reaction. Such an integrated unit opens the horizons for a direct

CO_2 to fuels/chemicals approach.

Keywords: CO_2 valorisation; RWGS; Fe catalysts; Cu promoter; integrated unit

1. Introduction

The rising atmospheric level of carbon dioxide (CO_2), as one of the major environmental issues, has caused global concern. On the basis of reported data, global CO_2 concentration reached around 405 ppm as of August 2018 [1]. However, the short-term problem is that the increasing trends in atmospheric carbon dioxide are at all inevitable due to the thriving development of industry and anthropologic activities. Therefore, we become increasingly aware of the importance of controlling “carbon footprint”.

With the development of science and technology, there have been several different methods proposed to reduce atmospheric CO_2. Carbon Capture and Storage (CCS) was first proposed as a means of captured CO_2 could be stored by geological, mineralization or oceanic means [2]. Although many researches focus on the scheme to reduce atmospheric carbon emissions via capture, a lot of progress needs to be made before it could be of practical use. A more attractive solution is Carbon Capture and Utilization (CCU), which aims to upgrade CO_2 to valuable fuels and other chemical products, such as methanol [3]. Another interesting product, which can be

further used to obtain fuels, is CO, which can be obtained from CO_2 through the RWGS reaction, and the Dry Reforming of Methane (DRM) as well as by photo-/electro-chemical processes.

Among the different methods for CO_2 utilisation, the RWGS reaction (Eq. (1)) is a promising route, as CO_2 is converted into CO which, together with H_2 forms syngas, which is well established as a useful chemical intermediate. Syngas, with various H_2:CO ratios, can be used as a precursor in chemical processes that produce chemicals such as methanol and long chain hydrocarbons such as diesel via the Fischer-Tropsch Synthesis (FTS). Besides, syngas can also be used as a hydrogen source to produce methane or ammonia.

$$CO_2 + H_2 \leftrightarrow CO + H_2O,\ \Delta H_{298}^0 = +42.1\,\mathrm{kJ/mol} \quad (1)$$

However, the operational conditions of the RWGS reaction reveal some challenges to develop this strategy. First, carbon dioxide is a highly stable molecule, and for its use as a reactant in this reaction, its high activation energy must be exceeded. Secondly, because of its endothermic nature, the RWGS reaction is thermodynamically favourable at high temperature. Furthermore, additional side reactions, such as CO methanation (Eq. (2)) and the Sabatier reaction (Eq. (3)), would occur under similar reaction conditions, consuming significant amounts of H_2. Therefore, not only high temperatures but also suitable catalysts are both required to obtain optimal CO_2 conversions and selectivity towards CO.

$$\mathrm{CO} + 3H_2 \leftrightarrow CH_4 + H_2O,\ \Delta H_{298}^0 = -206.5\,\mathrm{kJ/mol} \quad (2)$$

$$CO_2 + 4H_2 \leftrightarrow CH_4 + 2H_2O,\ \Delta H^0_{298} = -165.0\ \mathrm{kJ/mol} \quad (3)$$

It is known from previous studies that the selectivity of final products can be significantly influenced by the nature of active species in the catalyst. The formation of alcohols or hydrocarbons will compete with the CO production through the RWGS reaction. Beside selectivity, stability is another important factor to take into account in the catalyst performance. As high reaction temperatures are required, catalyst deactivation would occur during the RWGS reaction. This is mainly due to sintering of the active metal phase, and/or coke deposition [4, 5].

Thus, high-temperature endurable catalysts with considerable CO_2 conversion efficiency are required for the RWGS reaction. Additionally, from the perspective of the availability of the catalyst to large-scale applications, economically viable and abundant materials are more desirable.

Numerous catalysts, including noble metals [6-13] and transition metals as copper- [14-20], and nickel-based [6-11] catalysts have been studied for the RWGS reaction. It has been reported that this reaction is carried out at low temperatures over Cu-based catalysts. However, because of their poor thermal stability, these materials are not desirable for achieving high CO_2 conversion as they deactivate very easily. To improve the catalytic performance of copper-based catalysts at high temperature, researchers found that by adding a small amount of iron, their catalytic activity and stability can be remarkably enhanced [18]. For noble metal and nickel-based catalysts, one of the main problems is methanation [8, 12, 13, 21]. Kim et al. reported that

Pt/TiO_2 catalysts had significant catalytic performance advantages over Pt/Al_2O_3 in terms of activity and stability [22]. They found that the CO selectivity was dependent on the carbonate species which were the key intermediate present at reducible TiO_2 sites [23]. Recently, our team found that $Ni\text{-}FeO_X/CeO_2\text{-}Al_2O_3$ was an excellent catalyst for the RWGS reaction in terms of stability and selectivity towards CO [6]. By doping with Fe a reference $Ni/CeO_2\text{-}Al_2O_3$ catalyst a remarkable activity enhancement was observed due to the strong interaction between FeO_X and Ni atoms [6]. FeO_X facilitates Ni dispersion on the surface, and modifies its electronic properties leading to higher activity [6]. The support also plays a pivotal role in this reaction, particularly when oxygen they introduce oxygen mobility thus actively participating in the reaction mechanism [24]. From our previous study, the mixed framework of $Al_2O_3\text{-}Ce_2O_3$ boosted the redox properties of supported catalysts and provided a relatively large surface areas for active phase dispersion, thus improving the overall catalytic performance [6].

Based on further studies, iron-based catalysts are good for hydrogenation reactions of CO_2 due to its high oxygen mobility and its thermal stability [24, 25]. Weatherbee et al. [26] first reported that high levels of CO were produced over Fe/SiO_2 in CO_2 hydrogenation. However, Fe/SiO_2 performed relative low activity compared with other Group VIII metals. Promoters (like Cu, K, and Mo [27-34]) are often used with iron-based catalysts to improve the reaction rate and tune the selectivity to the desired product. Copper is often added to iron-based catalysts for Fischer-Tropsch (F-T) synthesis in order to enhance the catalyst reducibility of [28]. As for Fe-Mo

materials, Qin et al. showed improved dispersion of Fe species by Mo addition [32]. Besides, the Mo dispersing effect restrains the aggregation of active iron particles in the reaction [32]. Thus, addition of metals such as Ni, Cu and Mo seems an interesting approach in the study of Fe-based catalysts for the RWGS reaction. Furthermore, most studies of CO_2 hydrogenation on Fe-based catalysts focused on hydrocarbons or olefins' production through FTS [30, 35, 36]. However, the application of these systems to the RWGS have been studied in a lesser extension opening room for further advances on the catalysts design and process engineering.

In this scenario, we propose a series of novel multicomponent catalysts (Fe/CeO_2-Al_2O_3, Fe-Ni/CeO_2-Al_2O_3, Fe-Mo/CeO_2-Al_2O_3 and Fe-Cu/CeO_2-Al_2O_3) for gas phase CO_2 recycling. The prepared catalysts have been tested in the RWGS reaction and its competition with parallel processes such as methanation has been carefully addressed. A detailed characterisation study of the designed catalysts has been pursued to elucidate the main factors influencing the CO_2 conversion activity, aiming to showcase a successful strategy to develop highly effective and economically viable catalysts for CO_2 valorisation.

2. Experimental

2.1 Catalysts synthesis

The ceria-alumina support was synthesised by the wet impregnation method. The necessary amount of $Ce(NO_3)_3{\cdot}6H_2O$ (Sigma-Aldrich, absolute) to obtain 30 wt.% CeO_2 was dissolved in ethanol and added to PURALOX SCFa-230 alumina support

(Sasol, ≥99%). The excess of solvent was evaporated under reduced pressure, and the resulting solid was dried overnight and calcined at 500 ℃ for 4h. For Fe/CeAl, the necessary amount of $Fe(NO_3)_3 \cdot 9H_2O$ (Aldrich, ≥98%) was dissolved in ethanol to obtain 25 wt.% Fe_2O_3. Then home-made CeO_2-Al_2O_3 support was impregnated during 1 h in a rotary evaporator with the solution containing the metallic precursor. After that, solvent was removed by evaporation and the resultant slurry was dried and then calcined at 750 ℃ for 4 h.

The same procedure was used for the synthesis of FeNi/CeAl, FeMo/CeAl and FeCu/CeAl catalysts by sequential wet impregnation. First, the necessary amount of $Fe(NO_3)_3 \cdot 9H_2O$ (Aldrich, ≥98%) was dissolved in ethanol to obtain 15 wt.% Fe_2O_3. Then, the home-made CeO_2-Al_2O_3 support was impregnated with the solution containing the metallic precursor for 1 h in rotary evaporator. The resultant 15 wt.% Fe_2O_3 was equally divided, with each batch designated 10 wt.% of different second metal promoters. For each batch, the mass of $Ni(NO_3)_2 \cdot 6H_2O$, $Cu(NO_3)_2 \cdot 3H_2O$ and $(NH_4)_6 \cdot Mo_7O_{24} \cdot 4H_2O$ were added in ethanol solution (H_2O for MoO_X) to obtain 10 wt.% NiO, CuO or MoO_X as a second metal, respectively. After impregnation and solvent evaporation, all the samples were dried and then calcined at 750 ℃ for 4 h. In summary, we prepared five catalysts labelled as follow: Fe/CeAl, FeMo/CeAl, FeNi/CeAl and FeCu/CeAl, with equivalent amounts of metal loading.

2.2 Catalysts characterisation

X-Ray Diffraction (XRD) patterns were recorded on an X'Pert Pro PANalytical, using

Cu Kα radiation (40 mA, 45 kV) over a 2θ-range of 10-90° and a step size of 0.05° with a step time of 160 s.

X-Ray fluorescence (XRF) analysis was carried out on an EDAX Eagle III spectrophotometer, utilising rhodium as the radiation source.

The textural properties of catalysts were determined from N_2 adsorption–desorption isotherms recorded on a Micrometrics TriStar II 3020 apparatus (Norcross, GA, USA) at the boiling point of nitrogen (77 K). Prior to the adsorption–desorption measurements, the samples were degassed at 250 ℃ for 2 h under vacuum. The specific surface area was determined using the Brunauer–Emmett–Teller (BET) method, whilst average pore size and pore volume were obtained by the Barret–Joyner–Halenda (BJH) method.

H_2-TPR experiments were carried out in a U-shaped quartz reactor. 10% H_2/Ar reactive gas stream was passed through the catalyst with a total flow of 50 mL min^{-1}. A 10 ℃ min^{-1} heating rate was utilised to elevate from room temperature to 950 °C. Samples were treated with flowing Ar at 150 ℃ for 1 h before the TPR run. Hydrogen consumption was followed by on-line mass spectrometry (Pfeiffer, OmniStar GSD 301). Calibrated with a standard CuO reference (Sigma-Aldrich 99.99%)

XPS measurements were performed with a K-ALPHA spectrometer (Thermo Fisher Scientific, Waltham, MA, USA) operated in the constant energy mode with survey scan pass energies of 200 eV and narrow scan energies of 50 eV, to measure the whole energy band as well as selectively measure particular elements. All XPS

spectra were acquired using Al-Kα radiation (1486.6 eV) with a twin crystal monochromator, yielding a focused X-ray spot (elliptical in shape with a major axis length of 400 μm) at 3 mAx12 kV. Charge compensation was attained with the system flood gun, which provides low energy electrons and low energy argon ions from a single source. For the reference binding energy, the C1s core level was used, located at 284.6 eV. All samples were reduced ex-situ at 750 ℃ and, before recording the spectrum, the samples were maintained in the analysis chamber until a residual pressure of ca. 5×10^{-7} N/m^2 was reached.

2.3 Thermodynamic simulation

ChemStations' ChemCad software package was used to observe the thermodynamic limits of RWGS reaction over a range of temperatures, using a H_2/CO_2 ratio of 4:1. The Soave-Redlich-Kwong equation of state was used in a Gibbs reactor. Material flows into the reactor are identical to those intended to be used for experimentation. The results of these simulations are included in the catalytic performance plots.

2.4 Catalytic behaviour

For the catalytic runs, the catalyst was placed in a fixed bed continuous flow quartz reactor. Before any catalytic measurement, the catalyst was in situ reduced under a hydrogen flow (50 mL min^{-1} with a 1:4 ratio of H_2/N_2) at 750 ℃ for 1 h. Reaction products were analysed by on-line gas analyser (ABB AO2020 Advanced Optima Process Gas Analyser, ABB, Mannheim, Germany).

For the catalytic tests, each catalyst was evaluated within a temperature range of 400–750 ℃. The temperature was increased in 50 ℃ segments which were held for 30 mins with a heating rate between intervals of 10 ℃ min^{-1}. The reactants flow was held at a constant weight hourly space velocity (WHSV) of 30,000 mL g^{-1} h^{-1} with a H_2/CO_2 ratio of 4:1. For each test, 200 mg sample was used. The stability tests were measured at the same space velocity of 30,000 mL g^{-1} h^{-1} with a H_2/CO_2 ratio of 4:1 at 500 ℃ for 48 h.

The parameters used for measuring the catalytic activityof each sample in this work were CO_2 conversion (Eq. (4)), CO selectivity (Eq. (5)), and CH_4 selectivity (Eq. (6)) [30].

$$CO_2 \text{ conversion}(\%) = ([CO_2]_{In}-[CO_2]_{Out})/([CO_2]_{In})\times 100 \quad (4)$$

$$CO \text{ selectivity}(\%) = ([CO]_{Out})/([CO_2]_{In}-[CO_2]_{Out})\times 100 \quad (5)$$

$$CH_4 \text{ selectivity}(\%) = ([CH_4]_{Out})/([CO_2]_{In}-[CO_2]_{Out})\times 100 \quad (6)$$

Where $[CO_2]_{Out}$ and $[CH_4]_{Out}$ are the concentration of CO_2 and CH_4 in the outlet of the reactor and $[CO_2]_{In}$ is the CO_2 concentration in the initial gas mixture. The error in CO_2 conversion and CO/CH_4 selectivity for all the experiments is within ± 0.5%.

3. Results and discussion

3.1 XRF

Table 1 summarises the results of the actual composition of each catalyst from the XRF analysis. The results agree very well with the nominal values, indicating the

succeed preparation of the catalysts.

3.2 Textural properties

The N_2 adsorption-desorption isotherms are presented in Fig.1. All samples are mesoporous materials presenting a type IV isotherm according to the IUPAC classification. The textural properties of the catalysts are governed by the primary γ-alumina support.

Table 2 lists the surface area, pore volume, and average pore diameter of all calcined catalysts. As can be seen, the surface area of the bare support CeAl is around 162 m^2/g. The textural properties of the catalysts are governed by the primary γ-alumina support. Thus, the decrease of surface area and total pore volume after introduction of Fe and metal promoters can be related to partial covering the mesopores of the Al_2O_3 support, which is in a good agreement with previous findings [6]. Interestingly, among the dopants Mo seems to have the stronger effect in terms of surface area depletion but overall, we can consider that all the prepared catalysts are comparable in terms of textural properties.

3.3 XRD

Fig. 2 shows the XRD patterns for all the samples, including the bare CeO_2-Al_2O_3 support. The diffractogram of this material shows peaks at $2\theta = 37.6^o$, 39.5^o, 45.8^o, and 66.8^o attributed to the primary support γ-Al_2O_3 (JCPDS 00-048-0367); and diffraction peaks at $2\theta = 28.6^o$, 33^o, 47.5^o, 56.3^o, 59.1^o, 69.4^o, 76.7^o, 79.1^o, and 88.4^o

assigned to the fluorite-type CeO_2 cubic crystal structure (JCPDS 00-34-0394).

For all the four Fe-based calcined catalysts, in addition to the peaks attributed to the CeAl support, also peaks of hematite Fe_2O_3 at 24.1°, 33.3°, 35.7°, 41°, 49.5°, 54.2°, 62.3°, and 64.2° (JCPDS 00-001-1053) can be intuited. Some authors report that magnetite and maghemite present a cubic structure with very close lattice parameters, fact that makes it difficult to differentiate these structures even if both phases exhibit high crystallinity. However, in the XRD pattern associated with the maghemite phase there exist two additional peaks located at 24° (210) and 26.10° (211) [37]. On the other hand, the formation of $FeAl_2O_4$ spinel cannot be discarded [38], as will be discussed later on the H_2-TPR section. The diffraction peaks corresponding to the second metal oxide phases were not observed in the calcined catalysts, suggesting that Mo_xO_y, CuO_2 and NiO particles are small and well dispersed over the support. Previous works of our group reported that the presence of Fe in combination with other metal results in an enhanced dispersion, this supporting the absence of XRD reflections. [39]. Overall, this positive effect of improved dispersion in these samples could enhance the tolerance towards major culprits such as sintering [40].

In the case of the Ni-doped system, the presence of a Ni-Fe aluminate spinel should be taken into account. It is well accepted that the Ni loading is critical to fully form spinel under high calcination temperature during catalyst preparation [41]. The absence of NiO peaks in the X-Ray patterns could also be ascribed to the formation of Ni or Ni-Fe aluminate spinels, which coincides with the γ-Al_2O_3 (JCPDS 048-0367) at

37.58°, 45.76° and 66.79°, respectively [42]. The most likely situation is that surface $NiAl_2O_4$ spinel should co-exist with the γ-Al_2O_3 phase. Additionally, Kharaji et al. observed that Fe and Mo oxides can easily form Fe-Mo composite oxides (possibly as $Fe_2(MoO_4)_3$) after heat treatment, and this phase could remain in the structure of FeMo/CeAl catalyst during RWGS reaction due to the reduction-resistance of Fe-Mo composite oxides [43]. As reported by Qing *et al.* [32], only samples with Mo/Fe ratios greater than 25/100 can show the characteristic diffraction peaks of ferric molybdate, while the $Fe_2(MoO_4)_3$ phase may exist in an amorphous state in low Mo-loaded samples. Thus, this could be another reason for the absence in the diffractograms of the Mo-oxide phase in our FeMo/CeAl sample.

All samples were activated in hydrogen before reaction. In order to study our samples composition just before the RWGS reaction, reduced samples were characterized by XRD, and relevant information was extracted as also shown in Fig. 2. For all the catalysts, a new phase corresponding to metallic Fe was detected at 44.6°, 65.0°, 82.3° (JCPDS 01-087-0721) which confirms, at least, the partial reduction of Fe_2O_3. As can be seen in Fig. 2 b) and c), reduced samples containing Mo and Cu have basically the same patterns as the reference sample (Fe/CeAl). Cu-oxide phase is very likely fully reduced as per suggested elsewhere [44], but in the present study, the absence of peaks assigned to metallic Cu in the reduced FeCu/CeAl sample reflects the excellent dispersion of this promoter in this sample. For the FeMo/CeAl sample, as discussed, ferric molybdate could be formed during the treatment and maintained in amorphous state that may not be observed by XRD. For the FeNi/CeAl sample,

upon reduction, Fe_2O_3 diffraction peaks disappeared, while diffractions at 43.7^o and 51.5^o were obtained. According to previous studies, these two diffraction peaks can be assigned to Ni-Fe alloy (CAPES 26009) [45, 46]. The Ni-related diffraction shifts to an angle of 43.7°, lower than that for metallic Ni, is an indicative that Fe-Ni alloy can co-exist in this sample. It is reported that this alloy could be decomposed to Ni (44.5^o) and Fe_3O_4 (36^o, 43.5^o and 63^o) during the reaction [45], as we also observed and will be discussed later.

3.3 H_2-TPR

The H_2 temperature-programmed reduction was undertaken so the redox properties of the catalysts and the interactions between the metals and the support can be assessed. H_2-TPR results are shown in Fig. 3.

As can be seen, the TPR profiles of all calcined samples show a reduction zone at high temperature (around 880 ℃) that is associated to the reduction of bulk ceria [41] together with other species (Ni or Fe spinel) depending on the sample. In the profile of the Fe/CeAl, other two well-separated H_2 consumption peaks can be observed, which can be characteristic of the well-known two-stage reduction for iron oxide: the first stage at low temperature (400 ℃) represents the reduction of Fe_2O_3 to Fe_3O_4, whereas the second stage is attributed to the reduction of Fe_3O_4 to Fe^0 at higher temperature (650 ℃) [47]. According to previous studies, the second reduction peak (at higher temperature) is rather complex because the second reduction stage

involves the transformation of a mixture of Fe^{3+} and Fe^{2+} into Fe^0 (metallic iron phase) [48]. Furthermore, these broad peaks, apart to have a contribution from surface ceria reduction, are slightly shifted to lower temperatures due to Fe-Ce interactions. For the bimetallic catalysts, it is clear that the reduction of Fe species can be enhanced by addition of Cu species, resulting in an overall lowering of the reduction temperature. On the other hand, addition of Ni and Mo species seem to supress/hinder the overall reducibility of catalysts as compared with the monometallic one (Fe/CeAl).

The addition of Mo shifts the reduction peaks of FeO_x to higher temperature, which is consistent with results shown by Liu et al. [49], revealing hindered overall reducibility. In the present study, the pattern of Mo-containing sample shows three reduction zones, that could correspond to the reported following three reduction steps: $Fe_2(MoO_4)_3 \rightarrow FeMoO_4 + Mo_4O_{11} \rightarrow Fe_2Mo_3O_8 + Fe_3O_4 \rightarrow$ FeMo alloy [50]. The presence of the $Fe_2(MoO_4)_3$ phase was reported to inhibit to a certain extent the redox properties of iron-based catalysts [32]. Regarding our sample, certain metallic Fe is present in this Mo-Fe sample, as can be extracted from the XRD results.

As for the FeCu/CeAl catalyst, apart from the final reduction peak associated with the bulk ceria and Fe spinel, it shows three main reduction features. The lower temperature peaks at 200 ℃ and 350 ℃ can be attributed to the reduction of CuO (to Cu^0), and the possible partial Fe reduction due to Cu-Fe interaction [51-55]. Further reduction of the catalyst occurs at higher temperatures, around 500 ℃ and 900 ℃, accounting for Fe_2O_3 to Fe_3O_4, Fe_3O_4 to Fe^0 and the Fe spinel.

A reduction peak can be observed in high temperature region over the pattern of the FeNi/CeAl catalyst, but with broader range, starting from 650 ℃ to 900 ℃. This reduction peak can be assigned to the reduction of ceria and Ni and Fe spinel, which are hard to detect in XRD [56]. Furthermore, small peaks below to 650 ℃ can be observed, which could reveal the reduction of Ni and Fe oxides with different interactions (Fe-Ni-Ce) [57]. Fiuza et al. also suggested that Fe-Ni alloy would also be less reducible than the individual metals [46].

3.4 XPS

XPS is used to discern the surface composition and chemical status of the catalytic active species, since further clarification is needed in view of the complex H_2-TPR profiles obtained.

The Fe $2p_{3/2}$, Mo $3d_{5/2}$, Cu $2p_{3/2}$ and Ni $2p_{3/2}$ spectra of the reduced samples are represented in Fig. 4. Table 3 summarises the binding energies of the main peaks of each core-level. As can be seen from Fig. 4a, the analysis of the Fe $2p_{3/2}$ is quite complex. After the reduction treatment at 750 ℃ the spectra show that only a part of Fe was in the metallic state; therefore, different iron species (Fe, Fe_2O_3 and Fe_3O_4) co-exist in the surface of the reduced catalysts as it was already suggested by XRD results. In this way, for all catalysts the band around 705-707 eV is assigned to metallic Fe, while the band around 709-710 eV and 711-712 eV are characteristic of Fe^{2+} and Fe^{3+} respectively [6].

From Table 3, it can be seen that the peaks at a binding energy value of 709-710 eV,

have a higher contribution (%, deconvolution) indicating that Fe^{2+} from Fe_3O_4 ($Fe^{2+,3+}$) and FeO (Fe^{2+}) is likely to be the dominant state on the catalyst surface for all reduced catalysts. Indeed, other works have suggested that Fe_3O_4 (magnetite) is the active phase for WGS reaction [52, 58, 59], then we can expect that this phase may also facilitate the RWGS reaction.

Furthermore, it is worth noting that the binding energies of the Fe $2p_{3/2}$ level are influenced by the addition of the second metal, showing a slightly decrease of the electron density of Fe species due to the interactions between iron and the second metals. Thus, for the Ni- and Cu-doped samples, the stronger interaction between Fe and these metal promoters in comparission with other samples could influence the catalytic performance affecting the CO_2 adsorption, which is considered as the rate-limiting step in the RWGS reaction. In fact, it has been reported that the electron deficient state of Fe species enhance catalytic activity [32]

Fig.4 (b/c/d) also shows the Mo 3d, Cu 2p and Ni 2p XPS spectra of the second metals, respectively. For the Mo-doped sample, two peaks for Mo 3d XPS spectra can be obtained.The one with a binding energy of 227.9 eV is attributed to $Mo^{\varepsilon+\ (0\leq\varepsilon\leq2)}$ and the other with binding energy of 229.5 eV is identified as $Mo^{\delta+\ (2<\delta<4)}$ [60], corroborating that both H_2-TPR and XPS analysis of Mo-doped sample show a complicated redox process. For the Cu-doped sample, the Cu $2p_{3/2}$ spectrum for the reduced FeCu/CeAl catalysts shows two peaks around 932.4 eV and 934.0 eV, which are assigned to $Cu^{0,+1}$ copper and Cu^{2+} species [60].

Generally, the BE of metallic Ni 2p is 852.4 ± 0.4 eV, the BE of Ni 2p in NiO is 854 ± 0.4 eV, the BE of Ni 2p in $NiFe_2O_4$ is 855 ± 0.4 eV, and the BE of Ni 2p in $NiAl_2O_4$ is around 857 ± 0.4 eV [61]. For the FeNi/CeAl sample, the BE of Ni $2p_{3/2}$ are at 853.8 eV and 856.5 eV that could be assigned to NiO (Ni^{2+}) and $NiAl_2O_4$ (Ni^{2+}) respectively, but no presence of metallic Ni can be seen in reduced FeNi/CeAl [57]. These two observed binding energies of the Ni 2p peaks indicate the presence of interaction between Ni and Fe metal, and the interaction between Ni and Al_2O_3 support [62]. It is highly likely that during the reduction treatment, Fe-Ni alloy and $NiAl_2O_4$ are firstly formed, as also indicated by XRD results.

Furthermore an idea of the promoters dispersion on the catalysts' surface were estimated using Metal/Al ratios as shown in Table 3. As shown in the table the ratio varies as follows: Cu/Al > Mo/Al > Ni/Al indicating that Cu exposition in the surface is enhanced compared to that of Mo and Ni. This is indeed an interesting observation since Cu-species, including metallic Cu, Cu^{1+}, and Cu^{2+} have been proposed as active phase for this reaction [63].

3.5 Catalytic performance

3.5.1 Catalytic activity and selectivity

After understanding of the structural and electronic properties of the prepared catalysts, they were tested in the RWGS reaction to study their catalytic performances.

Firstly, the catalytic activity in terms of CO_2 conversion of the prepared catalysts is shown in Fig. 5(a), as well as the results of the thermodynamic simulation. Clearly, CO_2 conversion steadily increases with reaction temperature over all samples, reflecting the endothermic nature of the RWGS reaction.

All the promoted catalysts, except the Mo-doped one, display higher CO_2 conversion levels than the reference system Fe/CeAl. Indeed, the experimental results show that FeNi/CeAl exhibited the highest level of conversion in all the studied temperature range, followed by FeCu/CeAl. Interestingly, the FeMo/CeAl displayed significant lower conversion than the reference Fe/CeAl sample. This result evidences the XPS trends indicating that Mo has the weakest interaction with Fe among the studied promoters. As previously discussed, the Fe active phase for RWGS should be ideally an electronic deficient species. Ni- and Cu-doped catalysts reached CO_2 conversion levels rather close to the thermodynamic equilibrium. The improved catalytic performance of these two catalysts could be due the strong interaction between Fe and Ni/Cu, altering the electronic density of Fe and thus facilitating CO_2 activation on the catalytic surface, in good agreement with the XPS data. Along with the promotional effect on Fe, the presence of Ni and Cu helps the reaction due to their intrinsic activity for CO_2 reduction/hydrogenation processes [6, 18, 20, 42]. In other words, we can consider Cu and Ni not just as mere dopants but also as co-catalysts to boost the RWGS reaction. Indeed, it has been already reported that the addition of Cu in the catalysts would promote the reaction by adding up new active sites such as Fe-Cu ensembles and metallic Cu clusters [49, 64]. In our case this situation would be

further favoured due to the enhanced copper exposition in the catalyst's surface as per deduced from the XPS data.

In addition to CO_2 conversion, selectivity is another key factor when assessing the catalytic performance for RWGS reaction, especially at relative low reaction temperature due to the competitive process, CO_2 methanation. Thus, the selectivity profiles of CO/CH_4 *vs.* temperature were also compared over all Fe-based catalysts. The reference system, Fe/CeAl, shows good levels of CO selectivity even at low temperatures. Such trend is improved by the addition of Cu and Mo. Indeed, both Cu and Mo display practically full CO selectivity in the whole studied temperature range. Interestingly, the Ni promoted material (which was the best in terms of conversion) shows the poorest CO selectivity which is particularly poor in the low temperature range. The competition RWGS / CO_2 methanation is evident in this catalyst, being the later the dominant process in the low temperature window and limiting the applicability of this catalyst for a low-temperature RWGS unit. In summary, the addition of dopants has despair impact on the overall catalytic performance. On the one hand, Ni and Cu boost the CO_2 conversion due to the strong interaction with Fe which leads to Fe deficient species plus their intrinsic activity in the reaction acting as co-catalysts. Among these two systems, Ni is the best promoter in terms of CO_2 conversion. On the other hand, the nature of the added metals remarkable affects the selectivity. Herein Cu inhibits the methanation reaction resulting in a virtual full CO selectivity in the whole studied range. On the contrary Ni, due to its methanation capacity, shows poor selectivity towards the RWGS reaction in the medium-low temperature range.

Therefore, the FeCu/CeAl catalyst seems to be the best compromise to achieve the optimum activity/selectivity balance.

In order to discern changes happened on the crystalline structure of spent catalysts, a XRD study of the spent samples after the catalytic screening was accomplished (See Fig. 2). As it can be seen for the post-reaction samples, the metallic Fe phase contribution decreases after reaction, evidencing the oxidation of Fe towards the Fe_3O_4 phase. All XRD spent spectrum exhibited small peaks ascribed to Fe_3O_4, corresponding to the reflexions (220), (311), (400), (422), (511) and (440), which are similar to those reported before for Fe_3O_4 nanoparticles [65]. These results could be due to the oxidization of metallic iron by water formed during the chemical process. But either way, the presence of FeO_x plays an important role for the catalytic performance in terms of both CO_2 conversion and CO selectivity.

3.5.2 Long-term activity tests

For a real application of these catalysts in a CO_2 upgrading unit their long-term behaviour is of paramount importance. From Fig. 5, it is clear that Fe/CeAl and FeCu/CeAl exhibit the best activity/selectivity balance within the whole range of studied samples in terms of CO_2 conversion and CO selectivity. Furthermore, the FeNi/CeAl sample achieved the highest CO_2 conversion. These three samples were selected for the stability study, aiming to find further discrepancies between these three materials under continuous operation. The samples were studied far from equilibrium and at low temperature (500 ℃), since we are aim is to assess their

applicability in low-temperature RWGS unit.

Fig. 6 shows that CO_2 conversion remains approximately constant for the three samples, matching the CO_2 conversion level achieved in the catalytic screening experiments. The steady behaviour indicates excellent stability for long-term catalytic runs. Since the differences between the Fe/CeAl and FeCu/CeAl samples are no tvery notorious, the critical factor will be the CO selectivity for these samples. FeCu/CeAl reveals better catalytic performance regarding CO selectivity, which was over 99% during the whole experiment, while the CO selectivity was around 80% (and decreasing) and 65% for Fe/CeAl and FeNi/CeAl respectively. Therefore, the Cu-promoted Fe/CeAl catalyst is the catalyst of choice displaying an excellent catalytic performance in terms of activity/selective with outstanding selectivity for continuous operations. It is important to highlight the fact that this catalyst presents almost full selectivity towards CO at 500 ^{o}C, which is a relatively low reaction temperature where the CO_2 methanation process heavily competes with the RWGS [6]. This is a very important result from the process perspective. In particular, when the RWGS is coupled to a second unit such as F-T synthesis or a Methanol production reaction there is a big temperature gap between both reactors.

Typically, the RWGS reaction will run at high temperature range around 600-750 ℃ [6] and the second unit for FTS at 300-400 ℃ [30, 35, 66]. Our FeCu/CeAl catalyst can run in the 400-500 ℃ range with very high selectivity to CO, significantly decreasing the temperature gap between these two units. Thus, FeCu/CeAl brings a

great opportunity to facilitate the integration of the RWGS and the second upgrading unit to produce fuels and chemicals from CO_2.

Besides, further catalyst characterization supports the excellent results found in terms of stability. Post-stability XRD pattern of the three catalysts were obtained (Figure 7). It is clear that crystalline carbon species were not observed in the samples, indicating that carbon deposition is irrelevant under this reaction conditions for the prepared catalysts. This is mainly due to the excellent redox properties of CeO_2 in the support, as well as the prevention of metal sintering and subsequent carbon deposition [6]. Overall, the results corroborate the suitability of FeCu/CeAl for long runs with an excellent activity/stability/selectivity compromise.

4. Conclusions

The reverse water-gas shift reaction can be effectively catalysed by Fe-based catalysts supported on CeO_2-Al_2O_3. The addition of promoters such as Ni and Cu remarkably boost the CO_2 conversion capacity of these materials. The observed promotional effect is ascribed to the strong interaction between Fe and Ni/Cu, altering the electronic density of Fe and thus facilitating CO_2 activation on the catalytic surface, as revealed by XPS. In addition, Cu and Ni are not mere dopants for Fe but also, they can be regarded as co-catalysts due to their intrinsic activity in the reaction.

Different impact on the selectivity is also found when Cu and Ni are introduced in the catalyst's formulation. While the FeNi/CeO_2-Al_2O_3 catalyst favours CO_2 methanation, the FeCu/CeO_2-Al_2O_3 exhibit virtual full selectivity towards CO. Hence the Cu-doped

catalysts can be considered as the catalysts of choice for this reaction under the tested conditions. This sample also displays excellent performance for long-term operations, which makes it an appealing system for a real application.

Along with the excellent activity/selectivity/robustness form long-term runs trade-off demonstrated by the FeCu/CeO_2-Al_2O_3 catalyst, its uniqueness also relies on its high efficiency at medium-low temperatures. This is a very important result from the process perspective. If we envisaged an integrated process where the RWGS is coupled to a second unit such as F-T synthesis or a Methanol production reactor, our catalyst can help to overcome the temperature gap between the front and the end unit. In other words, our multicomponent catalyst represents a step ahead towards the development of CO_2 to fuels/chemicals units which will be essential in the modern low-carbon societies.

Acknowledgements

Financial support for this work was provided by the Department of Chemical and Process Engineering of the University of Surrey and the EPSRC grants EP/J020184/2 and EP/R512904/1 as well as the Royal Society Research Grant RSGR1180353. Authors would also like to acknowledge the Ministerio de Economía, Industrial Competitividad of Spain (Project MAT2016-80285-P). LPP also thanks Generalitat Valenciana for her postdoctoral fellow APOSTD2017.

References

1. NOAA. *Trends in Atmospheric Carbon Dioxide*. Global Greenhouse Gas Reference Network [cited 2018 01/12]; Available from: https://www.esrl.noaa.gov/gmd/ccgg/trends/.

2. UKRI. *Introduction to carbon capture and storage (CCS)*. How can CO_2 be stored? [cited 2018 18/09]; Available from: http://www.bgs.ac.uk/discoveringGeology/climateChange/CCS/home.html.

3. M. Mikkelsen, M. Jorgensen, and F.C. Krebs, *The teraton challenge: A review of fixation and transformation of carbon dioxide.* Energy Environ. Sci., 2010. **3**: p. 43-81.

4. P. Forzatti and L. Lietti, *Catalyst deactivation.* Catal. Today., 1999. **52**: p. 165-181.

5. J.G. Mccarty, et al., *Reactivity of Surface Carbon on Nickel Catalysts: Temperature-Programmed Surface Reaction with Hydrogen and Water*, in *In Coke Formation on Metal Surfaces*. 1983, American Chemical Society: Washington, DC. p. 253-282.

6. L. Yang, et al., *Highly efficient Ni/CeO_2 -Al_2O_3 catalysts for CO_2 upgrading via Reverse Water-Gas Shift: Effect of selected transition metal promoters.* Appl. Catal. B: Environ, 2018. **232**: p. 464-471.

7. K.A. Gharibi, S. Ahmad, and O. Mohammad, *Development of Ni-Mo/Al_2O_3 catalyst for reverse water gas shift (RWGS) reaction.* J. Nanosci. Nanotechnol., 2014. **14**: p. 6841-6847.

8. B.W. Lu and K. Kawamoto, *Preparation of monodispersed NiO particles in SBA-15, and its enhanced selectivity for reverse water gas shift reaction.* J. Environ. Chem. Eng., 2013. **1**.

9. B.W. Lu and K. Kawamoto, *Preparation of mesoporous CeO_2 and monodispersed NiO particles in CeO_2, and enhanced selectivity of NiO/CeO_2 for reverse water gas shift reaction.* Mater. Res. Bull., 2014. **53**: p. 70-78.

10. L.H. Wang, et al., *Effect of precipitants on Ni-CeO_2 catalysts prepared by a co-precipitation method for the reverse water-gas shift reaction.* J. Rare Earths., 2013. **31**: p. 969-974.

11. L.H. Wang, S.X. Liu, and Y. Liu, *Reverse water gas shift reaction over Co-precipitated Ni-CeO_2 catalysts.* J. Rare Earths., 2008. **26**: p. 66-70.

12. B.W. Lu and K. Kawamoto, *Preparation of the highly loaded and well-dispersed NiO/SBA-15 for methanation of producer gas.* J. Environ. Chem. Eng., 2013. **103**: p. 699-704.

13. L.H. Wang, et al., *Influence of preparation method on performance of Ni-CeO_2 catalysts for revese water-gas shift reaction.* J. Rare Earths., 2013. **31**: p. 559-564.

14. C.S. Chen and W.H. Cheng, *Study on the mechanism of CO formation in reverse water gas shift reaction over Cu/SiO_2 catalyst by pulse reaction, TPD and TPR.* Catal. Lett., 2002. **83**: p. 121-126.

15. C.S. Chen, et al., *Properties of Cu(thd)$_2$ as a Precursor to Prepare Cu/SiO_2 Catalyst Using the Atomic Layer Epitaxy Technique.* J. Am. Chem. Soc., 2006. **128**: p. 15950-15951.

16. C.S. Chen, J.H. Wu, and T.W. Lai, *Carbon Dioxide Hydrogenation on Cu Nanoparticles.* J. Phys. Chem. C., 2010. **114**: p. 15021-15028.

17. C.S. Chen, W.H. Cheng, and S.S. Lin, *Mechanism of CO formation in reverse water-gas shift reaction over Cu/Al_2O_3 catalyst.* Catal. Lett., 2000. **68**: p. 45-48.

18. C.S. Chen, W.H. Cheng, and S.S. Lin, *Enhanced activity and stability of a Cu/SiO_2 catalyst for the reverse water gas shift reaction by an iron promoter.* Chem. Commun., 2001: p. 1770–1771.

19. C.S. Chen, W.H. Cheng, and S.S. Lin, *Study of reverse water gas shift reaction by TPD, TPR and CO_2 hydrogenation over potassium-promoted Cu/SiO_2 catalyst.* Appl. Catal. A: Gen., 2003. **238**: p. 55-67.

20. C.S. Chen, W.H. Cheng, and S.S. Lin, *Study of iron-promoted Cu/SiO_2 catalyst on high temperature reverse water gas shift reaction.* Appl. Catal. A: Gen., 2004: p. 97-106.

21. F.V. Vázquez, et al., *Catalyst Screening and Kinetic Modeling for CO Production by High Pressure and Temperature Reverse Water Gas Shift for Fischer − Tropsch Applications.* Ind. Eng. Chem. Res., 2017. **56**: p. 13262 − 13272.

22. S.S. Kim, H.H. Lee, and S.C. Hong, *A study on the effect of support's reducibility on the reverse water-gas shift reaction over Pt catalysts.* Appl. Catal. A: Gen., 2012. **423-424**: p. 100-107.

23. S.S. Kim, K.H. Park, and S.C. Hong, *A study of the selectivity of the reverse water-gas shift reaction over Pt/TiO_2 catalysts.* Fuel. Processing. Technology., 2013. **108**.

24. Y.A. Daza and J.N. Kuhn, *CO_2 conversion by reverse water gas shift catalysis:*

comparision of catalysts, mechanisms and their consequences for CO_2 conversion to liquid fuels. RSC Adv., 2016. **6**: p. 49675-49691.

25. D.H. Kim, et al., *Reverse water gas shift reaction catalyzed by Fe nanoparticles with high catalytic activity and stability.* J. Ind. Eng. Chem., 2015. **23**: p. 67-71.

26. G. Weatherbee and C. Bartholomew, *Hydrogenation of CO_2 on Group VIII Metals.* J. Catal., 1983. **87**: p. 352-362.

27. H. Ando, et al., *Hydrocarbon synthesis from CO_2 over Fe-Cu catalysts.* Catal. Today., 1998. **45**.

28. S.R. Yan, et al., *Promotion effect of Fe-Cu catalyst for the hydrogenation of CO_2 and application to slurry reactor.* Appl. Catal. A: Gen., 2000. **194-195**: p. 63-70.

29. T. Riedel, et al., *Kinetics of CO_2 Hydrogenation on a K-Promoted Fe Catalyst.* Ind. Eng. Chem. Res., 2001. **40**: p. 1355-1363.

30. P.S. Sai Prasad, et al., *Fischer-Tropsch Synthesis by Carbon Dioxide Hydrogenation on Fe-Based Catalysts.* Catal. Surv. Asia., 2008. **12**: p. 170-183.

31. M.K. Gnanamani, et al., *Fischer–Tropsch synthesis: Effect of CO_2 containing syngas over Pt promoted Co/γ-Al_2O_3 and K-promoted Fe catalysts.* Catal. Commun., 2011. **12**: p. 936-939.

32. S.D. Qin, et al., *Fe-Mo interactions and their influence on Fischer-Tropsch synthesis performance.* Appl. Catal. A: Gen., 2011. **392**: p. 118-126.

33. J. Amelse, L. Schwartz, and J. Butt, *Iron alloy Fischer-Tropsch catalysts: III. Conversion dependence of selectivity and water-gas shift.* J. Catal., 1981. **72**: p. 95-110.

34. I.E. Wachs, D.J. Duyer, and E. Iglesia, *Characterizaiton of Fe, Fe-Cu, and Fe-Ag Fischer-Tropsch Catalysts.* Appl. Catal., 1984. **12**: p. 201-217.

35. J.H. Liu, et al., *Selectivity CO_2 Hydrogenation to Hydrocarbons on Cu-Promoted Fe-Based Catalysts: Dependence on Cu-Fe Interaction.* ACS Sustainable Chem. Eng., 2018. **6**: p. 10182-10190.

36. S. He, et al., *Carbon nanotube-supported bimetallic Cu-Fe catalysts for syngas conversion to higher alcohols.* Mol. Catal., 2019. **479**: p. 110610.

37. A.R. Baltazar, et al., *Effect of the Surfactant on the Growth and Oxidation of Iron Nanoparticles.* J. Nanomaterials, 2015. **2015**: p. 8.

38. A. Zaabout, et al., *Gas Switching Reforming (GSR) for syngas production with integrated CO_2 capture using iron-based oxygen carriers.* Inter. J. Greenhouse Gas Control, 2019. **63**: p. 175-183.

39. L. Pastor-Pérez, et al., *Synthetic natural gas production from CO_2 over Ni-x/CeO_2-ZrO_2 (x = Fe, Co) catalysts: Influence of promoters and space velocity.* Catal. Today., 2017. **317**: p. 108-113.

40. H.L. Lu, et al., *Metal (Fe, Co, Ce or La) doped nickel catalyst supported on ZrO_2 modified mesoporous clays for CO and CO_2 methanation.* Fuel., 2016. **183**: p. 335-344.

41. T. Stroud, et al., *Chemical CO_2 recycling via dry and bi reforming of methane using Ni-Sn/Al_2O_3 and Ni-Sn/CeO_2-Al_2O_3 catalysts.* Appl. Catal. B: Environ., 224. **224**: p. 125-135.

42. E. Le Sache, et al., *Multicomponent Ni-CeO_2 nanocatalysts for syngas production*

from CO_2/CH_4 mixtures. J. CO2 Util., 2018. **25**: p. 68-78.

43. A.G. Kharaji, A. Shariati, and M.A. Takassi, *A Novel γ-Alumina Support Fe-Mo Bimetallic Catalyst for Reverse Water Gas Shift Reaction.* Chin. J. Chem. Eng., 2013. **21**: p. 1007-1014.

44. L. Pastor-Pérez, et al., *CO_2 valorisation via Reverse Water-Gas Shift reaction using advanced Cs doped Fe-Cu/Al_2O_3 catalysts.* J. CO_2 Util., 2017. **21**: p. 423-428.

45. S. A. Theofanidis, et al., *Enhanced Carbon-Resistant Dry Reforming Fe-Ni Catalysts: Role of Fe.* ACS Catal., 2015. **5**.

46. R. da Paz Fiuza, M.A. da Silva, and J.S. Boaventura, *Development of Fe-Ni/YSZ-GDC electrocatalysts for application as SOFC anodes: XRD and TPR characterization and evaluation in the ethanol steam reforming reaction.* Int. J. Hydrogen Energy., 2010. **35**: p. 11216-11228.

47. L. Pastor-Pérez, et al., *Improving Fe/Al_2O_3 Catalysts for the Reverse Water-Gas Shift Reaction: On the Effect of Cs as Activity/Selectivity Promoter.* Catalysts., 2018. **8**.

48. H.J. Wan, et al., *Fischer-Tropsch Synthesis: Influence of Support Incorporation Manner on Metal Dispersion, Metal-Support Interaction, and Activities of Iron Catalysts.* ACS Catal., 2012. **2**: p. 1877-1883.

49. J.H. Liu, et al., *Selective CO_2 Hydrogenation to Hydrocarbons on Cu-Promoted FeBased Catalysts: Dependence on Cu−Fe Interaction.* ACS Sustainable Chem. Eng., 2018. **6**: p. 10182−10190.

50. H.L Zhang, J.Y. Shen, and X. Ge, *The Reduction Behavior of Fe-Mo-O Catalysts Studied by Temperature-Programmed Reduction Combined with in Situ Mössbauer*

Spectroscopy and X-Ray Diffraction. J. Solid State Chem., 1995. **117**: p. 127-135.

51. C. Martos, J. Dufour, and A. Ruiz, *Synthesis of Fe_3O_4-based catalysts for the high-temperaturewater gas shift reaction.* Int. J. Hydrogen Energy., 2009. **34**: p. 4475-4481.

52. L.Z. Zhang, et al., *Investigation of highly active Fe-Al-Cu catalysts for water-gas shift reaction.* Appl. Catal. A: Gen., 2008. **351**: p. 1-8.

53. L.Z Zhang, J.M. Millet, and U.S. Ozkan, *Effect of Cu loading on the catalytic performance of Fe–Al–Cu for water-gasshift reaction.* Appl. Catal. A: Gen., 2009. **357**: p. 66-72.

54. H. Zhang, et al., *Plasma-assisted preparation of Fe–Cu bimetal catalyst for higher alcoholssynthesis from carbon monoxide hydrogenation.* Fuel., 2010. **89**: p. 3127-3131.

55. T. Zhang, et al., *Selective catalytic reduction of NO with NH3 over HZSM-5-supported Fe–Cu nanocomposite catalysts: The Fe–Cu bimetallic effect.* 2014. **148-149**.

56. P.P. Li, et al., *The promotion effects of Ni on the properties of Cr/Al catalysts for propane dehydrogenation reaction.* Appl. Catal. A: Gen., 2016. **522**: p. 172-179.

57. J. Ashok and S. Kawi, *Nickel−Iron Alloy Supported over Iron−Alumina Catalysts for Steam Reforming of Biomass Tar Model Compound.* ACS Catal., 2014 **4**: p. 289−301.

58. S. Natesakhawat, et al., *Development of chromium-free iron-based catalysts for high-temperature water-gas shift reaction.* J. Molcata., 2006. **260**: p. 82-94.

59. D.W. Lee, et al., *The review of Cr-free Fe-based catalysts for high-temperature water-gas shift reactions.* Catal. Today., 2013. **210**: p. 2-9.

60. Q. Zhang, et al., *Understanding the promoter effect of Cu and Cs over highly effective β-Mo_2C catalysts for the reverse water-gas shift reaction.* Appl. Catal. B: Environ., 2019. **244**: p. 889-898.

61. C.D. Wanger, et al., *Handbook of X-ray Photoelectron Spectroscopy*. 1979, Minnesota. USA.: Perkin-Elmer Corp.

62. Z.L. Zhan and L. Zhao, *Electrochemical reduction of CO_2 in solid oxide electrolysis cells.* J. Pow. Sour., 2010. **195**: p. 7250-7254.

63. M. Estrella, et al., *In Situ Characterization of $CuFe_2O_4$ and Cu/Fe_3O_4 Water-Gas Shift Catalysts.* J. Phys. Chem. C., 2009. **113**: p. 14411–14417.

64. Z.H. Bao, W.Z. Ding, and Q. Li, *Effect of Fe/Cu ratio on the activity of Fe-Al-Cu catalysts for water gas shift reaction under hydrogen-rich atmosphere.* Int. J. Hydrogen Energy., 2012. **37**: p. 951-955.

65. K.S. Loh, et al., *Use of Fe_3O_4 Nanoparticles for Enhancement of Biosensor Response to the Herbicide 2,4-Dichlorophenoxyacetic Acid.* Sensors, 2008. **8 (9)**.

66. C.G. Visconti, et al., *CO_2 hydrogenation to hydrocarbons over Co and Fe-based Fischer-Tropsch catalysts.* Catal. Today., 2016. **277**.

CO_2 valorisation via Reverse Water-Gas Shift reaction using promoted Fe/CeO_2-Al_2O_3 catalysts: showcasing the potential of advanced catalysts to explore new processes design

L.Yang[1], L.Pastor-Pérez*[1,2], J.J.Villora-Pico[2], S.Gu[1], A.Sepúlveda-Escribano[2], T.R.Reina[1]

[1]*Chemical and Process Engineering Department, University of Surrey, Guildford, UK*

[2]*Laboratorio de Materiales Avanzados, Departamento de Química Inorgánica - Instituto Universitario de Materiales de Alicante Universidad de Alicante, Apartado 99, E-03080 Alicante, Spain.*

* corresponding authors: l.pastorperez@surrey.ac.uk

Abstract

The RWGS reaction represents a direct approach for gas-phase CO_2 upgrading. This work showcases the efficiency of Fe/CeO_2-Al_2O_3 catalysts for this process, and the effect of selected transition metal promoters such as Cu, Ni and Mo. Our results demonstrated that both Ni and Cu remarkably improved the performance of the monometallic Fe-catalyst. The competition Reverse Water-Gas Shift (RWGS) reaction/CO_2 methanation reaction was evident particularly for the Ni-catalyst, which displayed high selectivity to methane in the low-temperature range. Among the studied catalysts the Cu promoted sample represented the best choice, exhibiting the best activity/selectivity balance. In addition, the Cu-doped catalyst was very stable for long-term runs – an essential requisite for its implementation in flue gas upgrading units. This material can effectively catalyse the RWGS reaction at medium-low temperatures, providing the possibility to couple the RWGS reactor with a syngas conversion reaction. Such an integrated unit opens the horizons for a direct

CO_2 to fuels/chemicals approach.

Keywords: CO_2 valorisation; RWGS; Fe catalysts; Cu promoter; integrated unit

1. Introduction

The rising atmospheric level of carbon dioxide (CO_2), as one of the major environmental issues, has caused global concern. On the basis of reported data, global CO_2 concentration reached around 405 ppm as of August 2018 [1]. However, the short-term problem is that the increasing trends in atmospheric carbon dioxide are at all inevitable due to the thriving development of industry and anthropologic activities. Therefore, we become increasingly aware of the importance of controlling “carbon footprint”.

With the development of science and technology, there have been several different methods proposed to reduce atmospheric CO_2. Carbon Capture and Storage (CCS) was first proposed as a means of captured CO_2 could be stored by geological, mineralization or oceanic means [2]. Although many researches focus on the scheme to reduce atmospheric carbon emissions via capture, a lot of progress needs to be made before it could be of practical use. A more attractive solution is Carbon Capture and Utilization (CCU), which aims to upgrade CO_2 to valuable fuels and other chemical products, such as methanol [3]. Another interesting product, which can be

further used to obtain fuels, is CO, which can be obtained from CO_2 through the RWGS reaction, and the Dry Reforming of Methane (DRM) as well as by photo-/electro-chemical processes.

Among the different methods for CO_2 utilisation, the RWGS reaction (Eq. (1)) is a promising route, as CO_2 is converted into CO which, together with H_2 forms syngas, which is well established as a useful chemical intermediate. Syngas, with various H_2:CO ratios, can be used as a precursor in chemical processes that produce chemicals such as methanol and long chain hydrocarbons such as diesel via the Fischer-Tropsch Synthesis (FTS). Besides, syngas can also be used as a hydrogen source to produce methane or ammonia.

$$CO_2 + H_2 \leftrightarrow CO + H_2O, \ \Delta H^0_{298} = +42.1\,\mathrm{kJ/mol} \quad (1)$$

However, the operational conditions of the RWGS reaction reveal some challenges to develop this strategy. First, carbon dioxide is a highly stable molecule, and for its use as a reactant in this reaction, its high activation energy must be exceeded. Secondly, because of its endothermic nature, the RWGS reaction is thermodynamically favourable at high temperature. Furthermore, additional side reactions, such as CO methanation (Eq. (2)) and the Sabatier reaction (Eq. (3)), would occur under similar reaction conditions, consuming significant amounts of H_2. Therefore, not only high temperatures but also suitable catalysts are both required to obtain optimal CO_2 conversions and selectivity towards CO.

$$\mathrm{CO} + 3H_2 \leftrightarrow CH_4 + H_2O, \ \Delta H^0_{298} = -206.5\,\mathrm{kJ/mol} \quad (2)$$

$$CO_2 + 4H_2 \leftrightarrow CH_4 + 2H_2O,\ \Delta H^0_{298} = -165.0\ \mathrm{kJ/mol} \quad (3)$$

It is known from previous studies that the selectivity of final products can be significantly influenced by the nature of active species in the catalyst. The formation of alcohols or hydrocarbons will compete with the CO production through the RWGS reaction. Beside selectivity, stability is another important factor to take into account in the catalyst performance. As high reaction temperatures are required, catalyst deactivation would occur during the RWGS reaction. This is mainly due to sintering of the active metal phase, and/or coke deposition [4, 5].

Thus, high-temperature endurable catalysts with considerable CO_2 conversion efficiency are required for the RWGS reaction. Additionally, from the perspective of the availability of the catalyst to large-scale applications, economically viable and abundant materials are more desirable.

Numerous catalysts, including noble metals [6-13] and transition metals as copper- [14-20], and nickel-based [6-11] catalysts have been studied for the RWGS reaction. It has been reported that this reaction is carried out at low temperatures over Cu-based catalysts. However, because of their poor thermal stability, these materials are not desirable for achieving high CO_2 conversion as they deactivate very easily. To improve the catalytic performance of copper-based catalysts at high temperature, researchers found that by adding a small amount of iron, their catalytic activity and stability can be remarkably enhanced [18]. For noble metal and nickel-based catalysts, one of the main problems is methanation [8, 12, 13, 21]. Kim et al. reported that

Pt/TiO_2 catalysts had significant catalytic performance advantages over Pt/Al_2O_3 in terms of activity and stability [22]. They found that the CO selectivity was dependent on the carbonate species which were the key intermediate present at reducible TiO_2 sites [23]. Recently, our team found that $Ni\text{-}FeO_X/CeO_2\text{-}Al_2O_3$ was an excellent catalyst for the RWGS reaction in terms of stability and selectivity towards CO [6]. By doping with Fe a reference $Ni/CeO_2\text{-}Al_2O_3$ catalyst a remarkable activity enhancement was observed due to the strong interaction between FeO_X and Ni atoms [6]. FeO_X facilitates Ni dispersion on the surface, and modifies its electronic properties leading to higher activity [6]. The support also plays a pivotal role in this reaction, particularly when oxygen they introduce oxygen mobility thus actively participating in the reaction mechanism [24]. From our previous study, the mixed framework of $Al_2O_3\text{-}Ce_2O_3$ boosted the redox properties of supported catalysts and provided a relatively large surface areas for active phase dispersion, thus improving the overall catalytic performance [6].

Based on further studies, iron-based catalysts are good for hydrogenation reactions of CO_2 due to its high oxygen mobility and its thermal stability [24, 25]. Weatherbee et al. [26] first reported that high levels of CO were produced over Fe/SiO_2 in CO_2 hydrogenation. However, Fe/SiO_2 performed relative low activity compared with other Group VIII metals. Promoters (like Cu, K, and Mo [27-34]) are often used with iron-based catalysts to improve the reaction rate and tune the selectivity to the desired product. Copper is often added to iron-based catalysts for Fischer-Tropsch (F-T) synthesis in order to enhance the catalyst reducibility of [28]. As for Fe-Mo

materials, Qin et al. showed improved dispersion of Fe species by Mo addition [32]. Besides, the Mo dispersing effect restrains the aggregation of active iron particles in the reaction [32]. Thus, addition of metals such as Ni, Cu and Mo seems an interesting approach in the study of Fe-based catalysts for the RWGS reaction. Furthermore, most studies of CO_2 hydrogenation on Fe-based catalysts focused on hydrocarbons or olefins' production through FTS [30, 35, 36]. However, the application of these systems to the RWGS have been studied in a lesser extension opening room for further advances on the catalysts design and process engineering.

In this scenario, we propose a series of novel multicomponent catalysts (Fe/CeO_2-Al_2O_3, Fe-Ni/CeO_2-Al_2O_3, Fe-Mo/CeO_2-Al_2O_3 and Fe-Cu/CeO_2-Al_2O_3) for gas phase CO_2 recycling. The prepared catalysts have been tested in the RWGS reaction and its competition with parallel processes such as methanation has been carefully addressed. A detailed characterisation study of the designed catalysts has been pursued to elucidate the main factors influencing the CO_2 conversion activity, aiming to showcase a successful strategy to develop highly effective and economically viable catalysts for CO_2 valorisation.

2. Experimental

2.1 Catalysts synthesis

The ceria-alumina support was synthesised by the wet impregnation method. The necessary amount of $Ce(NO_3)_3{\cdot}6H_2O$ (Sigma-Aldrich, absolute) to obtain 30 wt.% CeO_2 was dissolved in ethanol and added to PURALOX SCFa-230 alumina support

(Sasol, ≥99%). The excess of solvent was evaporated under reduced pressure, and the resulting solid was dried overnight and calcined at 500 ℃ for 4h. For Fe/CeAl, the necessary amount of $Fe(NO_3)_3 \cdot 9H_2O$ (Aldrich, ≥98%) was dissolved in ethanol to obtain 25 wt.% Fe_2O_3. Then home-made CeO_2-Al_2O_3 support was impregnated during 1 h in a rotary evaporator with the solution containing the metallic precursor. After that, solvent was removed by evaporation and the resultant slurry was dried and then calcined at 750 ℃ for 4 h.

The same procedure was used for the synthesis of FeNi/CeAl, FeMo/CeAl and FeCu/CeAl catalysts by sequential wet impregnation. First, the necessary amount of $Fe(NO_3)_3 \cdot 9H_2O$ (Aldrich, ≥98%) was dissolved in ethanol to obtain 15 wt.% Fe_2O_3. Then, the home-made CeO_2-Al_2O_3 support was impregnated with the solution containing the metallic precursor for 1 h in rotary evaporator. The resultant 15 wt.% Fe_2O_3 was equally divided, with each batch designated 10 wt.% of different second metal promoters. For each batch, the mass of $Ni(NO_3)_2 \cdot 6H_2O$, $Cu(NO_3)_2 \cdot 3H_2O$ and $(NH_4)_6 \cdot Mo_7O_{24} \cdot 4H_2O$ were added in ethanol solution (H_2O for MoO_X) to obtain 10 wt.% NiO, CuO or MoO_X as a second metal, respectively. After impregnation and solvent evaporation, all the samples were dried and then calcined at 750 ℃ for 4 h. In summary, we prepared five catalysts labelled as follow: Fe/CeAl, FeMo/CeAl, FeNi/CeAl and FeCu/CeAl, with equivalent amounts of metal loading.

2.2 Catalysts characterisation

X-Ray Diffraction (XRD) patterns were recorded on an X'Pert Pro PANalytical, using

Cu Kα radiation (40 mA, 45 kV) over a 2θ-range of 10-90° and a step size of 0.05° with a step time of 160 s.

X-Ray fluorescence (XRF) analysis was carried out on an EDAX Eagle III spectrophotometer, utilising rhodium as the radiation source.

The textural properties of catalysts were determined from N_2 adsorption–desorption isotherms recorded on a Micrometrics TriStar II 3020 apparatus (Norcross, GA, USA) at the boiling point of nitrogen (77 K). Prior to the adsorption–desorption measurements, the samples were degassed at 250 ℃ for 2 h under vacuum. The specific surface area was determined using the Brunauer–Emmett–Teller (BET) method, whilst average pore size and pore volume were obtained by the Barret–Joyner–Halenda (BJH) method.

H_2-TPR experiments were carried out in a U-shaped quartz reactor. 10% H_2/Ar reactive gas stream was passed through the catalyst with a total flow of 50 mL min^{-1}. A 10 ℃ min^{-1} heating rate was utilised to elevate from room temperature to 950 °C. Samples were treated with flowing Ar at 150 ℃ for 1 h before the TPR run. Hydrogen consumption was followed by on-line mass spectrometry (Pfeiffer, OmniStar GSD 301). Calibrated with a standard CuO reference (Sigma-Aldrich 99.99%)

XPS measurements were performed with a K-ALPHA spectrometer (Thermo Fisher Scientific, Waltham, MA, USA) operated in the constant energy mode with survey scan pass energies of 200 eV and narrow scan energies of 50 eV, to measure the whole energy band as well as selectively measure particular elements. All XPS

spectra were acquired using Al-Kα radiation (1486.6 eV) with a twin crystal monochromator, yielding a focused X-ray spot (elliptical in shape with a major axis length of 400 µm) at 3 mAx12 kV. Charge compensation was attained with the system flood gun, which provides low energy electrons and low energy argon ions from a single source. For the reference binding energy, the C1s core level was used, located at 284.6 eV. All samples were reduced ex-situ at 750 ℃ and, before recording the spectrum, the samples were maintained in the analysis chamber until a residual pressure of ca. 5×10^{-7} N/m^2 was reached.

2.3 Thermodynamic simulation

ChemStations' ChemCad software package was used to observe the thermodynamic limits of RWGS reaction over a range of temperatures, using a H_2/CO_2 ratio of 4:1. The Soave-Redlich-Kwong equation of state was used in a Gibbs reactor. Material flows into the reactor are identical to those intended to be used for experimentation. The results of these simulations are included in the catalytic performance plots.

2.4 Catalytic behaviour

For the catalytic runs, the catalyst was placed in a fixed bed continuous flow quartz reactor. Before any catalytic measurement, the catalyst was in situ reduced under a hydrogen flow (50 mL min^{-1} with a 1:4 ratio of H_2/N_2) at 750 ℃ for 1 h. Reaction products were analysed by on-line gas analyser (ABB AO2020 Advanced Optima Process Gas Analyser, ABB, Mannheim, Germany).

For the catalytic tests, each catalyst was evaluated within a temperature range of 400–750 ℃. The temperature was increased in 50 ℃ segments which were held for 30 mins with a heating rate between intervals of 10 ℃ min^{-1}. The reactants flow was held at a constant weight hourly space velocity (WHSV) of 30,000 mL g^{-1} h^{-1} with a H_2/CO_2 ratio of 4:1. For each test, 200 mg sample was used. The stability tests were measured at the same space velocity of 30,000 mL g^{-1} h^{-1} with a H_2/CO_2 ratio of 4:1 at 500 ℃ for 48 h.

The parameters used for measuring the catalytic activityof each sample in this work were CO_2 conversion (Eq. (4)), CO selectivity (Eq. (5)), and CH_4 selectivity (Eq. (6)) [30].

$$CO_2 \text{ conversion}(\%) = ([CO_2]_{In}-[CO_2]_{Out})/([CO_2]_{In})\times 100 \quad (4)$$

$$CO \text{ selectivity}(\%) = ([CO]_{Out})/([CO_2]_{In}-[CO_2]_{Out})\times 100 \quad (5)$$

$$CH_4 \text{ selectivity}(\%) = ([CH_4]_{Out})/([CO_2]_{In}-[CO_2]_{Out})\times 100 \quad (6)$$

Where $[CO_2]_{Out}$ and $[CH_4]_{Out}$ are the concentration of CO_2 and CH_4 in the outlet of the reactor and $[CO_2]_{In}$ is the CO_2 concentration in the initial gas mixture. The error in CO_2 conversion and CO/CH_4 selectivity for all the experiments is within ± 0.5%.

3. Results and discussion

3.1 XRF

Table 1 summarises the results of the actual composition of each catalyst from the XRF analysis. The results agree very well with the nominal values, indicating the

succeed preparation of the catalysts.

3.2 Textural properties

The N_2 adsorption-desorption isotherms are presented in Fig.1. All samples are mesoporous materials presenting a type IV isotherm according to the IUPAC classification. The textural properties of the catalysts are governed by the primary γ-alumina support.

Table 2 lists the surface area, pore volume, and average pore diameter of all calcined catalysts. As can be seen, the surface area of the bare support CeAl is around 162 m^2/g. The textural properties of the catalysts are governed by the primary γ-alumina support. Thus, the decrease of surface area and total pore volume after introduction of Fe and metal promoters can be related to partial covering the mesopores of the Al_2O_3 support, which is in a good agreement with previous findings [6]. Interestingly, among the dopants Mo seems to have the stronger effect in terms of surface area depletion but overall, we can consider that all the prepared catalysts are comparable in terms of textural properties.

3.3 XRD

Fig. 2 shows the XRD patterns for all the samples, including the bare CeO_2-Al_2O_3 support. The diffractogram of this material shows peaks at 2θ = 37.6^o, 39.5^o, 45.8^o, and 66.8^o attributed to the primary support γ-Al_2O_3 (JCPDS 00-048-0367); and diffraction peaks at 2θ = 28.6^o, 33^o, 47.5^o, 56.3^o, 59.1^o, 69.4 ^{o}, 76.7^o, 79.1^o, and 88.4^o

assigned to the fluorite-type CeO_2 cubic crystal structure (JCPDS 00-34-0394).

For all the four Fe-based calcined catalysts, in addition to the peaks attributed to the CeAl support, also peaks of hematite Fe_2O_3 at 24.1°, 33.3°, 35.7°, 41°, 49.5°, 54.2°, 62.3°, and 64.2° (JCPDS 00-001-1053) can be intuited. Some authors report that magnetite and maghemite present a cubic structure with very close lattice parameters, fact that makes it difficult to differentiate these structures even if both phases exhibit high crystallinity. However, in the XRD pattern associated with the maghemite phase there exist two additional peaks located at 24° (210) and 26.10° (211) [37]. On the other hand, the formation of $FeAl_2O_4$ spinel cannot be discarded [38], as will be discussed later on the H_2-TPR section. The diffraction peaks corresponding to the second metal oxide phases were not observed in the calcined catalysts, suggesting that Mo_xO_y, CuO_2 and NiO particles are small and well dispersed over the support. Previous works of our group reported that the presence of Fe in combination with other metal results in an enhanced dispersion, this supporting the absence of XRD reflections. [39]. Overall, this positive effect of improved dispersion in these samples could enhance the tolerance towards major culprits such as sintering [40].

In the case of the Ni-doped system, the presence of a Ni-Fe aluminate spinel should be taken into account. It is well accepted that the Ni loading is critical to fully form spinel under high calcination temperature during catalyst preparation [41]. The absence of NiO peaks in the X-Ray patterns could also be ascribed to the formation of Ni or Ni-Fe aluminate spinels, which coincides with the γ-Al_2O_3 (JCPDS 048-0367) at

37.58°, 45.76° and 66.79°, respectively [42]. The most likely situation is that surface $NiAl_2O_4$ spinel should co-exist with the γ-Al_2O_3 phase. Additionally, Kharaji et al. observed that Fe and Mo oxides can easily form Fe-Mo composite oxides (possibly as $Fe_2(MoO_4)_3$) after heat treatment, and this phase could remain in the structure of FeMo/CeAl catalyst during RWGS reaction due to the reduction-resistance of Fe-Mo composite oxides [43]. As reported by Qing *et al.* [32], only samples with Mo/Fe ratios greater than 25/100 can show the characteristic diffraction peaks of ferric molybdate, while the $Fe_2(MoO_4)_3$ phase may exist in an amorphous state in low Mo-loaded samples. Thus, this could be another reason for the absence in the diffractograms of the Mo-oxide phase in our FeMo/CeAl sample.

All samples were activated in hydrogen before reaction. In order to study our samples composition just before the RWGS reaction, reduced samples were characterized by XRD, and relevant information was extracted as also shown in Fig. 2. For all the catalysts, a new phase corresponding to metallic Fe was detected at 44.6°, 65.0°, 82.3° (JCPDS 01-087-0721) which confirms, at least, the partial reduction of Fe_2O_3. As can be seen in Fig. 2 b) and c), reduced samples containing Mo and Cu have basically the same patterns as the reference sample (Fe/CeAl). Cu-oxide phase is very likely fully reduced as per suggested elsewhere [44], but in the present study, the absence of peaks assigned to metallic Cu in the reduced FeCu/CeAl sample reflects the excellent dispersion of this promoter in this sample. For the FeMo/CeAl sample, as discussed, ferric molybdate could be formed during the treatment and maintained in amorphous state that may not be observed by XRD. For the FeNi/CeAl sample,

upon reduction, Fe_2O_3 diffraction peaks disappeared, while diffractions at 43.7^o and 51.5^o were obtained. According to previous studies, these two diffraction peaks can be assigned to Ni-Fe alloy (CAPES 26009) [45, 46]. The Ni-related diffraction shifts to an angle of 43.7°, lower than that for metallic Ni, is an indicative that Fe-Ni alloy can co-exist in this sample. It is reported that this alloy could be decomposed to Ni (44.5^o) and Fe_3O_4 (36^o, 43.5^o and 63^o) during the reaction [45], as we also observed and will be discussed later.

3.3 H_2-TPR

The H_2 temperature-programmed reduction was undertaken so the redox properties of the catalysts and the interactions between the metals and the support can be assessed. H_2-TPR results are shown in Fig. 3.

As can be seen, the TPR profiles of all calcined samples show a reduction zone at high temperature (around 880 ℃) that is associated to the reduction of bulk ceria [41] together with other species (Ni or Fe spinel) depending on the sample. In the profile of the Fe/CeAl, other two well-separated H_2 consumption peaks can be observed, which can be characteristic of the well-known two-stage reduction for iron oxide: the first stage at low temperature (400 ℃) represents the reduction of Fe_2O_3 to Fe_3O_4, whereas the second stage is attributed to the reduction of Fe_3O_4 to Fe^0 at higher temperature (650 ℃) [47]. According to previous studies, the second reduction peak (at higher temperature) is rather complex because the second reduction stage

involves the transformation of a mixture of Fe^{3+} and Fe^{2+} into Fe^0 (metallic iron phase) [48]. Furthermore, these broad peaks, apart to have a contribution from surface ceria reduction, are slightly shifted to lower temperatures due to Fe-Ce interactions. For the bimetallic catalysts, it is clear that the reduction of Fe species can be enhanced by addition of Cu species, resulting in an overall lowering of the reduction temperature. On the other hand, addition of Ni and Mo species seem to supress/hinder the overall reducibility of catalysts as compared with the monometallic one (Fe/CeAl).

The addition of Mo shifts the reduction peaks of FeO_x to higher temperature, which is consistent with results shown by Liu et al. [49], revealing hindered overall reducibility. In the present study, the pattern of Mo-containing sample shows three reduction zones, that could correspond to the reported following three reduction steps: $Fe_2(MoO_4)_3 \rightarrow FeMoO_4 + Mo_4O_{11} \rightarrow Fe_2Mo_3O_8 + Fe_3O_4 \rightarrow$ FeMo alloy [50]. The presence of the $Fe_2(MoO_4)_3$ phase was reported to inhibit to a certain extent the redox properties of iron-based catalysts [32]. Regarding our sample, certain metallic Fe is present in this Mo-Fe sample, as can be extracted from the XRD results.

As for the FeCu/CeAl catalyst, apart from the final reduction peak associated with the bulk ceria and Fe spinel, it shows three main reduction features. The lower temperature peaks at 200 ℃ and 350 ℃ can be attributed to the reduction of CuO (to Cu^0), and the possible partial Fe reduction due to Cu-Fe interaction [51-55]. Further reduction of the catalyst occurs at higher temperatures, around 500 ℃ and 900 ℃, accounting for Fe_2O_3 to Fe_3O_4, Fe_3O_4 to Fe^0 and the Fe spinel.

A reduction peak can be observed in high temperature region over the pattern of the FeNi/CeAl catalyst, but with broader range, starting from 650 ℃ to 900 ℃. This reduction peak can be assigned to the reduction of ceria and Ni and Fe spinel, which are hard to detect in XRD [56]. Furthermore, small peaks below to 650 ℃ can be observed, which could reveal the reduction of Ni and Fe oxides with different interactions (Fe-Ni-Ce) [57]. Fiuza et al. also suggested that Fe-Ni alloy would also be less reducible than the individual metals [46].

3.4 XPS

XPS is used to discern the surface composition and chemical status of the catalytic active species, since further clarification is needed in view of the complex H_2-TPR profiles obtained.

The Fe $2p_{3/2}$, Mo $3d_{5/2}$, Cu $2p_{3/2}$ and Ni $2p_{3/2}$ spectra of the reduced samples are represented in Fig. 4. Table 3 summarises the binding energies of the main peaks of each core-level. As can be seen from Fig. 4a, the analysis of the Fe $2p_{3/2}$ is quite complex. After the reduction treatment at 750 ℃ the spectra show that only a part of Fe was in the metallic state; therefore, different iron species (Fe, Fe_2O_3 and Fe_3O_4) co-exist in the surface of the reduced catalysts as it was already suggested by XRD results. In this way, for all catalysts the band around 705-707 eV is assigned to metallic Fe, while the band around 709-710 eV and 711-712 eV are characteristic of Fe^{2+} and Fe^{3+} respectively [6].

From Table 3, it can be seen that the peaks at a binding energy value of 709-710 eV,

have a higher contribution (%, deconvolution) indicating that Fe^{2+} from Fe_3O_4 ($Fe^{2+,3+}$) and FeO (Fe^{2+}) is likely to be the dominant state on the catalyst surface for all reduced catalysts. Indeed, other works have suggested that Fe_3O_4 (magnetite) is the active phase for WGS reaction [52, 58, 59], then we can expect that this phase may also facilitate the RWGS reaction.

Furthermore, it is worth noting that the binding energies of the Fe $2p_{3/2}$ level are influenced by the addition of the second metal, showing a slightly decrease of the electron density of Fe species due to the interactions between iron and the second metals. Thus, for the Ni- and Cu-doped samples, the stronger interaction between Fe and these metal promoters in comparission with other samples could influence the catalytic performance affecting the CO_2 adsorption, which is considered as the rate-limiting step in the RWGS reaction. In fact, it has been reported that the electron deficient state of Fe species enhance catalytic activity [32]

Fig.4 (b/c/d) also shows the Mo 3d, Cu 2p and Ni 2p XPS spectra of the second metals, respectively. For the Mo-doped sample, two peaks for Mo 3d XPS spectra can be obtained.The one with a binding energy of 227.9 eV is attributed to $Mo^{\varepsilon+\ (0\leq\varepsilon\leq2)}$ and the other with binding energy of 229.5 eV is identified as $Mo^{\delta+\ (2<\delta<4)}$ [60], corroborating that both H_2-TPR and XPS analysis of Mo-doped sample show a complicated redox process. For the Cu-doped sample, the Cu $2p_{3/2}$ spectrum for the reduced FeCu/CeAl catalysts shows two peaks around 932.4 eV and 934.0 eV, which are assigned to $Cu^{0,+1}$ copper and Cu^{2+} species [60].

Generally, the BE of metallic Ni 2p is 852.4 ± 0.4 eV, the BE of Ni 2p in NiO is 854 ± 0.4 eV, the BE of Ni 2p in $NiFe_2O_4$ is 855 ± 0.4 eV, and the BE of Ni 2p in $NiAl_2O_4$ is around 857 ± 0.4 eV [61]. For the FeNi/CeAl sample, the BE of Ni $2p_{3/2}$ are at 853.8 eV and 856.5 eV that could be assigned to NiO (Ni^{2+}) and $NiAl_2O_4$ (Ni^{2+}) respectively, but no presence of metallic Ni can be seen in reduced FeNi/CeAl [57]. These two observed binding energies of the Ni 2p peaks indicate the presence of interaction between Ni and Fe metal, and the interaction between Ni and Al_2O_3 support [62]. It is highly likely that during the reduction treatment, Fe-Ni alloy and $NiAl_2O_4$ are firstly formed, as also indicated by XRD results.

Furthermore an idea of the promoters dispersion on the catalysts' surface were estimated using Metal/Al ratios as shown in Table 3. As shown in the table the ratio varies as follows: Cu/Al > Mo/Al > Ni/Al indicating that Cu exposition in the surface is enhanced compared to that of Mo and Ni. This is indeed an interesting observation since Cu-species, including metallic Cu, Cu^{1+}, and Cu^{2+} have been proposed as active phase for this reaction [63].

3.5 Catalytic performance

3.5.1 Catalytic activity and selectivity

After understanding of the structural and electronic properties of the prepared catalysts, they were tested in the RWGS reaction to study their catalytic performances.

Firstly, the catalytic activity in terms of CO_2 conversion of the prepared catalysts is shown in Fig. 5(a), as well as the results of the thermodynamic simulation. Clearly, CO_2 conversion steadily increases with reaction temperature over all samples, reflecting the endothermic nature of the RWGS reaction.

All the promoted catalysts, except the Mo-doped one, display higher CO_2 conversion levels than the reference system Fe/CeAl. Indeed, the experimental results show that FeNi/CeAl exhibited the highest level of conversion in all the studied temperature range, followed by FeCu/CeAl. Interestingly, the FeMo/CeAl displayed significant lower conversion than the reference Fe/CeAl sample. This result evidences the XPS trends indicating that Mo has the weakest interaction with Fe among the studied promoters. As previously discussed, the Fe active phase for RWGS should be ideally an electronic deficient species. Ni- and Cu-doped catalysts reached CO_2 conversion levels rather close to the thermodynamic equilibrium. The improved catalytic performance of these two catalysts could be due the strong interaction between Fe and Ni/Cu, altering the electronic density of Fe and thus facilitating CO_2 activation on the catalytic surface, in good agreement with the XPS data. Along with the promotional effect on Fe, the presence of Ni and Cu helps the reaction due to their intrinsic activity for CO_2 reduction/hydrogenation processes [6, 18, 20, 42]. In other words, we can consider Cu and Ni not just as mere dopants but also as co-catalysts to boost the RWGS reaction. Indeed, it has been already reported that the addition of Cu in the catalysts would promote the reaction by adding up new active sites such as Fe-Cu ensembles and metallic Cu clusters [49, 64]. In our case this situation would be

further favoured due to the enhanced copper exposition in the catalyst's surface as per deduced from the XPS data.

In addition to CO_2 conversion, selectivity is another key factor when assessing the catalytic performance for RWGS reaction, especially at relative low reaction temperature due to the competitive process, CO_2 methanation. Thus, the selectivity profiles of CO/CH_4 *vs.* temperature were also compared over all Fe-based catalysts. The reference system, Fe/CeAl, shows good levels of CO selectivity even at low temperatures. Such trend is improved by the addition of Cu and Mo. Indeed, both Cu and Mo display practically full CO selectivity in the whole studied temperature range. Interestingly, the Ni promoted material (which was the best in terms of conversion) shows the poorest CO selectivity which is particularly poor in the low temperature range. The competition RWGS / CO_2 methanation is evident in this catalyst, being the later the dominant process in the low temperature window and limiting the applicability of this catalyst for a low-temperature RWGS unit. In summary, the addition of dopants has despair impact on the overall catalytic performance. On the one hand, Ni and Cu boost the CO_2 conversion due to the strong interaction with Fe which leads to Fe deficient species plus their intrinsic activity in the reaction acting as co-catalysts. Among these two systems, Ni is the best promoter in terms of CO_2 conversion. On the other hand, the nature of the added metals remarkable affects the selectivity. Herein Cu inhibits the methanation reaction resulting in a virtual full CO selectivity in the whole studied range. On the contrary Ni, due to its methanation capacity, shows poor selectivity towards the RWGS reaction in the medium-low temperature range.

Therefore, the FeCu/CeAl catalyst seems to be the best compromise to achieve the optimum activity/selectivity balance.

In order to discern changes happened on the crystalline structure of spent catalysts, a XRD study of the spent samples after the catalytic screening was accomplished (See Fig. 2). As it can be seen for the post-reaction samples, the metallic Fe phase contribution decreases after reaction, evidencing the oxidation of Fe towards the Fe_3O_4 phase. All XRD spent spectrum exhibited small peaks ascribed to Fe_3O_4, corresponding to the reflexions (220), (311), (400), (422), (511) and (440), which are similar to those reported before for Fe_3O_4 nanoparticles [65]. These results could be due to the oxidization of metallic iron by water formed during the chemical process. But either way, the presence of FeO_x plays an important role for the catalytic performance in terms of both CO_2 conversion and CO selectivity.

3.5.2 Long-term activity tests

For a real application of these catalysts in a CO_2 upgrading unit their long-term behaviour is of paramount importance. From Fig. 5, it is clear that Fe/CeAl and FeCu/CeAl exhibit the best activity/selectivity balance within the whole range of studied samples in terms of CO_2 conversion and CO selectivity. Furthermore, the FeNi/CeAl sample achieved the highest CO_2 conversion. These three samples were selected for the stability study, aiming to find further discrepancies between these three materials under continuous operation. The samples were studied far from equilibrium and at low temperature (500 °C), since we are aim is to assess their

applicability in low-temperature RWGS unit.

Fig. 6 shows that CO_2 conversion remains approximately constant for the three samples, matching the CO_2 conversion level achieved in the catalytic screening experiments. The steady behaviour indicates excellent stability for long-term catalytic runs. Since the differences between the Fe/CeAl and FeCu/CeAl samples are no tvery notorious, the critical factor will be the CO selectivity for these samples. FeCu/CeAl reveals better catalytic performance regarding CO selectivity, which was over 99% during the whole experiment, while the CO selectivity was around 80% (and decreasing) and 65% for Fe/CeAl and FeNi/CeAl respectively. Therefore, the Cu-promoted Fe/CeAl catalyst is the catalyst of choice displaying an excellent catalytic performance in terms of activity/selective with outstanding selectivity for continuous operations. It is important to highlight the fact that this catalyst presents almost full selectivity towards CO at 500 ^{o}C, which is a relatively low reaction temperature where the CO_2 methanation process heavily competes with the RWGS [6]. This is a very important result from the process perspective. In particular, when the RWGS is coupled to a second unit such as F-T synthesis or a Methanol production reaction there is a big temperature gap between both reactors.

Typically, the RWGS reaction will run at high temperature range around 600-750 ℃ [6] and the second unit for FTS at 300-400 ℃ [30, 35, 66]. Our FeCu/CeAl catalyst can run in the 400-500 ℃ range with very high selectivity to CO, significantly decreasing the temperature gap between these two units. Thus, FeCu/CeAl brings a

great opportunity to facilitate the integration of the RWGS and the second upgrading unit to produce fuels and chemicals from CO_2.

Besides, further catalyst characterization supports the excellent results found in terms of stability. Post-stability XRD pattern of the three catalysts were obtained (Figure 7). It is clear that crystalline carbon species were not observed in the samples, indicating that carbon deposition is irrelevant under this reaction conditions for the prepared catalysts. This is mainly due to the excellent redox properties of CeO_2 in the support, as well as the prevention of metal sintering and subsequent carbon deposition [6]. Overall, the results corroborate the suitability of FeCu/CeAl for long runs with an excellent activity/stability/selectivity compromise.

4. Conclusions

The reverse water-gas shift reaction can be effectively catalysed by Fe-based catalysts supported on CeO_2-Al_2O_3. The addition of promoters such as Ni and Cu remarkably boost the CO_2 conversion capacity of these materials. The observed promotional effect is ascribed to the strong interaction between Fe and Ni/Cu, altering the electronic density of Fe and thus facilitating CO_2 activation on the catalytic surface, as revealed by XPS. In addition, Cu and Ni are not mere dopants for Fe but also, they can be regarded as co-catalysts due to their intrinsic activity in the reaction.

Different impact on the selectivity is also found when Cu and Ni are introduced in the catalyst's formulation. While the FeNi/CeO_2-Al_2O_3 catalyst favours CO_2 methanation, the FeCu/CeO_2-Al_2O_3 exhibit virtual full selectivity towards CO. Hence the Cu-doped

catalysts can be considered as the catalysts of choice for this reaction under the tested conditions. This sample also displays excellent performance for long-term operations, which makes it an appealing system for a real application.

Along with the excellent activity/selectivity/robustness form long-term runs trade-off demonstrated by the FeCu/CeO_2-Al_2O_3 catalyst, its uniqueness also relies on its high efficiency at medium-low temperatures. This is a very important result from the process perspective. If we envisaged an integrated process where the RWGS is coupled to a second unit such as F-T synthesis or a Methanol production reactor, our catalyst can help to overcome the temperature gap between the front and the end unit. In other words, our multicomponent catalyst represents a step ahead towards the development of CO_2 to fuels/chemicals units which will be essential in the modern low-carbon societies.

Acknowledgements

Financial support for this work was provided by the Department of Chemical and Process Engineering of the University of Surrey and the EPSRC grants EP/J020184/2 and EP/R512904/1 as well as the Royal Society Research Grant RSGR1180353. Authors would also like to acknowledge the Ministerio de Economía, Industrial Competitividad of Spain (Project MAT2016-80285-P). LPP also thanks Generalitat Valenciana for her postdoctoral fellow APOSTD2017.

References

1. NOAA. *Trends in Atmospheric Carbon Dioxide*. Global Greenhouse Gas Reference Network [cited 2018 01/12]; Available from: https://www.esrl.noaa.gov/gmd/ccgg/trends/.

2. UKRI. *Introduction to carbon capture and storage (CCS)*. How can CO_2 be stored? [cited 2018 18/09]; Available from: http://www.bgs.ac.uk/discoveringGeology/climateChange/CCS/home.html.

3. M. Mikkelsen, M. Jorgensen, and F.C. Krebs, *The teraton challenge: A review of fixation and transformation of carbon dioxide.* Energy Environ. Sci., 2010. **3**: p. 43-81.

4. P. Forzatti and L. Lietti, *Catalyst deactivation.* Catal. Today., 1999. **52**: p. 165-181.

5. J.G. Mccarty, et al., *Reactivity of Surface Carbon on Nickel Catalysts: Temperature-Programmed Surface Reaction with Hydrogen and Water*, in *In Coke Formation on Metal Surfaces*. 1983, American Chemical Society: Washington, DC. p. 253-282.

6. L. Yang, et al., *Highly efficient Ni/CeO_2 -Al_2O_3 catalysts for CO_2 upgrading via Reverse Water-Gas Shift: Effect of selected transition metal promoters.* Appl. Catal. B: Environ, 2018. **232**: p. 464-471.

7. K.A. Gharibi, S. Ahmad, and O. Mohammad, *Development of Ni-Mo/Al_2O_3 catalyst for reverse water gas shift (RWGS) reaction.* J. Nanosci. Nanotechnol., 2014. **14**: p. 6841-6847.

8. B.W. Lu and K. Kawamoto, *Preparation of monodispersed NiO particles in SBA-15, and its enhanced selectivity for reverse water gas shift reaction.* J. Environ. Chem. Eng., 2013. **1**.

9. B.W. Lu and K. Kawamoto, *Preparation of mesoporous CeO_2 and monodispersed NiO particles in CeO_2, and enhanced selectivity of NiO/CeO_2 for reverse water gas shift reaction.* Mater. Res. Bull., 2014. **53**: p. 70-78.

10. L.H. Wang, et al., *Effect of precipitants on Ni-CeO_2 catalysts prepared by a co-precipitation method for the reverse water-gas shift reaction.* J. Rare Earths., 2013. **31**: p. 969-974.

11. L.H. Wang, S.X. Liu, and Y. Liu, *Reverse water gas shift reaction over Co-precipitated Ni-CeO_2 catalysts.* J. Rare Earths., 2008. **26**: p. 66-70.

12. B.W. Lu and K. Kawamoto, *Preparation of the highly loaded and well-dispersed NiO/SBA-15 for methanation of producer gas.* J. Environ. Chem. Eng., 2013. **103**: p. 699-704.

13. L.H. Wang, et al., *Influence of preparation method on performance of Ni-CeO_2 catalysts for revese water-gas shift reaction.* J. Rare Earths., 2013. **31**: p. 559-564.

14. C.S. Chen and W.H. Cheng, *Study on the mechanism of CO formation in reverse water gas shift reaction over Cu/SiO_2 catalyst by pulse reaction, TPD and TPR.* Catal. Lett., 2002. **83**: p. 121-126.

15. C.S. Chen, et al., *Properties of Cu(thd)$_2$ as a Precursor to Prepare Cu/SiO_2 Catalyst Using the Atomic Layer Epitaxy Technique.* J. Am. Chem. Soc., 2006. **128**: p. 15950-15951.

16. C.S. Chen, J.H. Wu, and T.W. Lai, *Carbon Dioxide Hydrogenation on Cu Nanoparticles.* J. Phys. Chem. C., 2010. **114**: p. 15021-15028.

17. C.S. Chen, W.H. Cheng, and S.S. Lin, *Mechanism of CO formation in reverse water-gas shift reaction over Cu/Al_2O_3 catalyst.* Catal. Lett., 2000. **68**: p. 45-48.

18. C.S. Chen, W.H. Cheng, and S.S. Lin, *Enhanced activity and stability of a Cu/SiO_2 catalyst for the reverse water gas shift reaction by an iron promoter.* Chem. Commun., 2001: p. 1770–1771.

19. C.S. Chen, W.H. Cheng, and S.S. Lin, *Study of reverse water gas shift reaction by TPD, TPR and CO_2 hydrogenation over potassium-promoted Cu/SiO_2 catalyst.* Appl. Catal. A: Gen., 2003. **238**: p. 55-67.

20. C.S. Chen, W.H. Cheng, and S.S. Lin, *Study of iron-promoted Cu/SiO_2 catalyst on high temperature reverse water gas shift reaction.* Appl. Catal. A: Gen., 2004: p. 97-106.

21. F.V. Vázquez, et al., *Catalyst Screening and Kinetic Modeling for CO Production by High Pressure and Temperature Reverse Water Gas Shift for Fischer − Tropsch Applications.* Ind. Eng. Chem. Res., 2017. **56**: p. 13262 − 13272.

22. S.S. Kim, H.H. Lee, and S.C. Hong, *A study on the effect of support's reducibility on the reverse water-gas shift reaction over Pt catalysts.* Appl. Catal. A: Gen., 2012. **423-424**: p. 100-107.

23. S.S. Kim, K.H. Park, and S.C. Hong, *A study of the selectivity of the reverse water-gas shift reaction over Pt/TiO_2 catalysts.* Fuel. Processing. Technology., 2013. **108**.

24. Y.A. Daza and J.N. Kuhn, *CO_2 conversion by reverse water gas shift catalysis:*

comparision of catalysts, mechanisms and their consequences for CO_2 conversion to liquid fuels. RSC Adv., 2016. **6**: p. 49675-49691.

25. D.H. Kim, et al., *Reverse water gas shift reaction catalyzed by Fe nanoparticles with high catalytic activity and stability.* J. Ind. Eng. Chem., 2015. **23**: p. 67-71.

26. G. Weatherbee and C. Bartholomew, *Hydrogenation of CO_2 on Group VIII Metals.* J. Catal., 1983. **87**: p. 352-362.

27. H. Ando, et al., *Hydrocarbon synthesis from CO_2 over Fe-Cu catalysts.* Catal. Today., 1998. **45**.

28. S.R. Yan, et al., *Promotion effect of Fe-Cu catalyst for the hydrogenation of CO_2 and application to slurry reactor.* Appl. Catal. A: Gen., 2000. **194-195**: p. 63-70.

29. T. Riedel, et al., *Kinetics of CO_2 Hydrogenation on a K-Promoted Fe Catalyst.* Ind. Eng. Chem. Res., 2001. **40**: p. 1355-1363.

30. P.S. Sai Prasad, et al., *Fischer-Tropsch Synthesis by Carbon Dioxide Hydrogenation on Fe-Based Catalysts.* Catal. Surv. Asia., 2008. **12**: p. 170-183.

31. M.K. Gnanamani, et al., *Fischer–Tropsch synthesis: Effect of CO_2 containing syngas over Pt promoted Co/γ-Al_2O_3 and K-promoted Fe catalysts.* Catal. Commun., 2011. **12**: p. 936-939.

32. S.D. Qin, et al., *Fe-Mo interactions and their influence on Fischer-Tropsch synthesis performance.* Appl. Catal. A: Gen., 2011. **392**: p. 118-126.

33. J. Amelse, L. Schwartz, and J. Butt, *Iron alloy Fischer-Tropsch catalysts: III. Conversion dependence of selectivity and water-gas shift.* J. Catal., 1981. **72**: p. 95-110.

34. I.E. Wachs, D.J. Duyer, and E. Iglesia, *Characterizaiton of Fe, Fe-Cu, and Fe-Ag Fischer-Tropsch Catalysts.* Appl. Catal., 1984. **12**: p. 201-217.

35. J.H. Liu, et al., *Selectivity CO_2 Hydrogenation to Hydrocarbons on Cu-Promoted Fe-Based Catalysts: Dependence on Cu-Fe Interaction.* ACS Sustainable Chem. Eng., 2018. **6**: p. 10182-10190.

36. S. He, et al., *Carbon nanotube-supported bimetallic Cu-Fe catalysts for syngas conversion to higher alcohols.* Mol. Catal., 2019. **479**: p. 110610.

37. A.R. Baltazar, et al., *Effect of the Surfactant on the Growth and Oxidation of Iron Nanoparticles.* J. Nanomaterials, 2015. **2015**: p. 8.

38. A. Zaabout, et al., *Gas Switching Reforming (GSR) for syngas production with integrated CO_2 capture using iron-based oxygen carriers.* Inter. J. Greenhouse Gas Control, 2019. **63**: p. 175-183.

39. L. Pastor-Pérez, et al., *Synthetic natural gas production from CO_2 over Ni-x/CeO_2-ZrO_2 (x = Fe, Co) catalysts: Influence of promoters and space velocity.* Catal. Today., 2017. **317**: p. 108-113.

40. H.L. Lu, et al., *Metal (Fe, Co, Ce or La) doped nickel catalyst supported on ZrO_2 modified mesoporous clays for CO and CO_2 methanation.* Fuel., 2016. **183**: p. 335-344.

41. T. Stroud, et al., *Chemical CO_2 recycling via dry and bi reforming of methane using Ni-Sn/Al_2O_3 and Ni-Sn/CeO_2-Al_2O_3 catalysts.* Appl. Catal. B: Environ., 224. **224**: p. 125-135.

42. E. Le Sache, et al., *Multicomponent Ni-CeO_2 nanocatalysts for syngas production*

from CO_2/CH_4 mixtures. J. CO2 Util., 2018. **25**: p. 68-78.

43. A.G. Kharaji, A. Shariati, and M.A. Takassi, *A Novel γ-Alumina Support Fe-Mo Bimetallic Catalyst for Reverse Water Gas Shift Reaction.* Chin. J. Chem. Eng., 2013. **21**: p. 1007-1014.

44. L. Pastor-Pérez, et al., *CO_2 valorisation via Reverse Water-Gas Shift reaction using advanced Cs doped Fe-Cu/Al_2O_3 catalysts.* J. CO_2 Util., 2017. **21**: p. 423-428.

45. S. A. Theofanidis, et al., *Enhanced Carbon-Resistant Dry Reforming Fe-Ni Catalysts: Role of Fe.* ACS Catal., 2015. **5**.

46. R. da Paz Fiuza, M.A. da Silva, and J.S. Boaventura, *Development of Fe-Ni/YSZ-GDC electrocatalysts for application as SOFC anodes: XRD and TPR characterization and evaluation in the ethanol steam reforming reaction.* Int. J. Hydrogen Energy., 2010. **35**: p. 11216-11228.

47. L. Pastor-Pérez, et al., *Improving Fe/Al_2O_3 Catalysts for the Reverse Water-Gas Shift Reaction: On the Effect of Cs as Activity/Selectivity Promoter.* Catalysts., 2018. **8**.

48. H.J. Wan, et al., *Fischer-Tropsch Synthesis: Influence of Support Incorporation Manner on Metal Dispersion, Metal-Support Interaction, and Activities of Iron Catalysts.* ACS Catal., 2012. **2**: p. 1877-1883.

49. J.H. Liu, et al., *Selective CO_2 Hydrogenation to Hydrocarbons on Cu-Promoted FeBased Catalysts: Dependence on Cu−Fe Interaction.* ACS Sustainable Chem. Eng., 2018. **6**: p. 10182−10190.

50. H.L Zhang, J.Y. Shen, and X. Ge, *The Reduction Behavior of Fe-Mo-O Catalysts Studied by Temperature-Programmed Reduction Combined with in Situ Mössbauer*

Spectroscopy and X-Ray Diffraction. J. Solid State Chem., 1995. **117**: p. 127-135.

51. C. Martos, J. Dufour, and A. Ruiz, *Synthesis of Fe_3O_4-based catalysts for the high-temperaturewater gas shift reaction.* Int. J. Hydrogen Energy., 2009. **34**: p. 4475-4481.

52. L.Z. Zhang, et al., *Investigation of highly active Fe-Al-Cu catalysts for water-gas shift reaction.* Appl. Catal. A: Gen., 2008. **351**: p. 1-8.

53. L.Z Zhang, J.M. Millet, and U.S. Ozkan, *Effect of Cu loading on the catalytic performance of Fe–Al–Cu for water-gasshift reaction.* Appl. Catal. A: Gen., 2009. **357**: p. 66-72.

54. H. Zhang, et al., *Plasma-assisted preparation of Fe–Cu bimetal catalyst for higher alcoholssynthesis from carbon monoxide hydrogenation.* Fuel., 2010. **89**: p. 3127-3131.

55. T. Zhang, et al., *Selective catalytic reduction of NO with NH3 over HZSM-5-supported Fe–Cu nanocomposite catalysts: The Fe–Cu bimetallic effect.* 2014. **148-149**.

56. P.P. Li, et al., *The promotion effects of Ni on the properties of Cr/Al catalysts for propane dehydrogenation reaction.* Appl. Catal. A: Gen., 2016. **522**: p. 172-179.

57. J. Ashok and S. Kawi, *Nickel−Iron Alloy Supported over Iron−Alumina Catalysts for Steam Reforming of Biomass Tar Model Compound.* ACS Catal., 2014 **4**: p. 289−301.

58. S. Natesakhawat, et al., *Development of chromium-free iron-based catalysts for high-temperature water-gas shift reaction.* J. Molcata., 2006. **260**: p. 82-94.

59. D.W. Lee, et al., *The review of Cr-free Fe-based catalysts for high-temperature water-gas shift reactions.* Catal. Today., 2013. **210**: p. 2-9.

60. Q. Zhang, et al., *Understanding the promoter effect of Cu and Cs over highly effective β-Mo_2C catalysts for the reverse water-gas shift reaction.* Appl. Catal. B: Environ., 2019. **244**: p. 889-898.

61. C.D. Wanger, et al., *Handbook of X-ray Photoelectron Spectroscopy*. 1979, Minnesota. USA.: Perkin-Elmer Corp.

62. Z.L. Zhan and L. Zhao, *Electrochemical reduction of CO_2 in solid oxide electrolysis cells.* J. Pow. Sour., 2010. **195**: p. 7250-7254.

63. M. Estrella, et al., *In Situ Characterization of $CuFe_2O_4$ and Cu/Fe_3O_4 Water-Gas Shift Catalysts.* J. Phys. Chem. C., 2009. **113**: p. 14411–14417.

64. Z.H. Bao, W.Z. Ding, and Q. Li, *Effect of Fe/Cu ratio on the activity of Fe-Al-Cu catalysts for water gas shift reaction under hydrogen-rich atmosphere.* Int. J. Hydrogen Energy., 2012. **37**: p. 951-955.

65. K.S. Loh, et al., *Use of Fe_3O_4 Nanoparticles for Enhancement of Biosensor Response to the Herbicide 2,4-Dichlorophenoxyacetic Acid.* Sensors, 2008. **8 (9)**.

66. C.G. Visconti, et al., *CO_2 hydrogenation to hydrocarbons over Co and Fe-based Fischer-Tropsch catalysts.* Catal. Today., 2016. **277**.

Table

Table 1. XRF characterisation results.

Catalysts	Composition (w/w%)		
	CeO_2	Fe_2O_3	Mo_2O_3/NiO/CuO
Fe/CeAl	33.4	16.2	-
FeMo/CeAl	30.7	14.3	11.8
FeNi/CeAl	30.6	15.4	10.0
FeCu/CeAl	31.3	15.3	9.4

Table 2. Textural properties of the prepared catalysts.

Catalysts	BET (m^2/g)	Total Pore Volume (cm^3/g)	Pore size (nm)
CeAl	162	0.35	8.3
Fe/CeAl	88	0.25	10.3
FeMo/CeAl	70	0.24	12.8
FeCu/CeAl	80	0.23	8.8
FeNi/CeAl	86	0.23	8.0

Table 3. Binding energies of the Fe $2p_{3/2}$, Mo $3d_{5/2}$, Cu $2p_{3/2}$, and Ni $2p_{3/2}$ core-levels in the reduced catalysts, and proportion of Fe species.

Catalysts	Fe $2p_{3/2}$ (eV)			Cu $2p_{3/2}$ (eV)		Mo $3d_{5/2}$ (eV)		Ni $2p_{3/2}$ (eV)		2nd metal/Al (at./at.)
	Fe	**Fe^{2+}**	**Fe^{3+}**	**$Cu^{0,+1}$**	**Cu^{2+}**	**$Mo^{\varepsilon+}$**	**$Mo^{\delta+}$**	**Ni^{2+}**	**$NiAl_2O_4$**	
Fe/CeAl	706.7 (17%)	709.7 (60%)	711.8 (23%)	-	-	-	-	-	-	-
FeCu/CeAl	706.8 (26%)	709.8 (42%)	712.1 (32%)	932.4	934.0	-	-	-	-	**Cu/Al** 0.097
FeMo/CeAl	706.0 (28%)	709.2 (48%)	711.2 (24%)	-	-	227.9	229.3	-	-	**Mo/Al** 0.024
FeNi/CeAl	707.0 (26%)	710.1 (48%)	712.2 (26%)	-	-	-	-	853.8	856.5	**Ni/Al** 0.010

* $0 \leq \varepsilon \leq 2$
* $2 < \delta < 4$

Figure

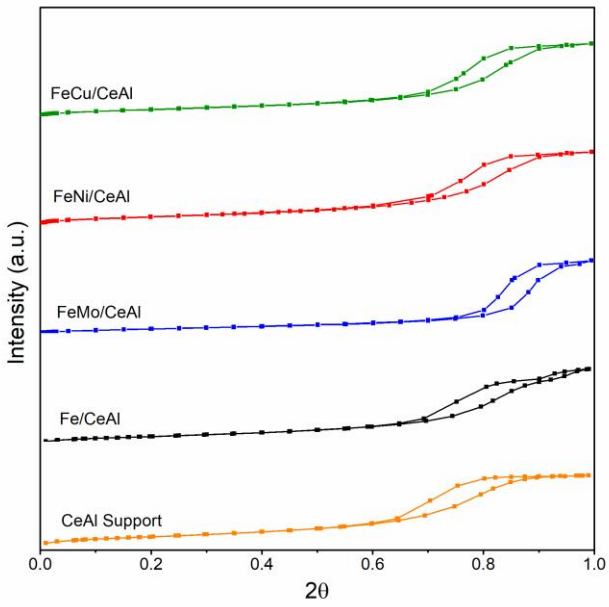

Fig. 1 N_2 adsorption-desorption isotherms of the calcined samples.

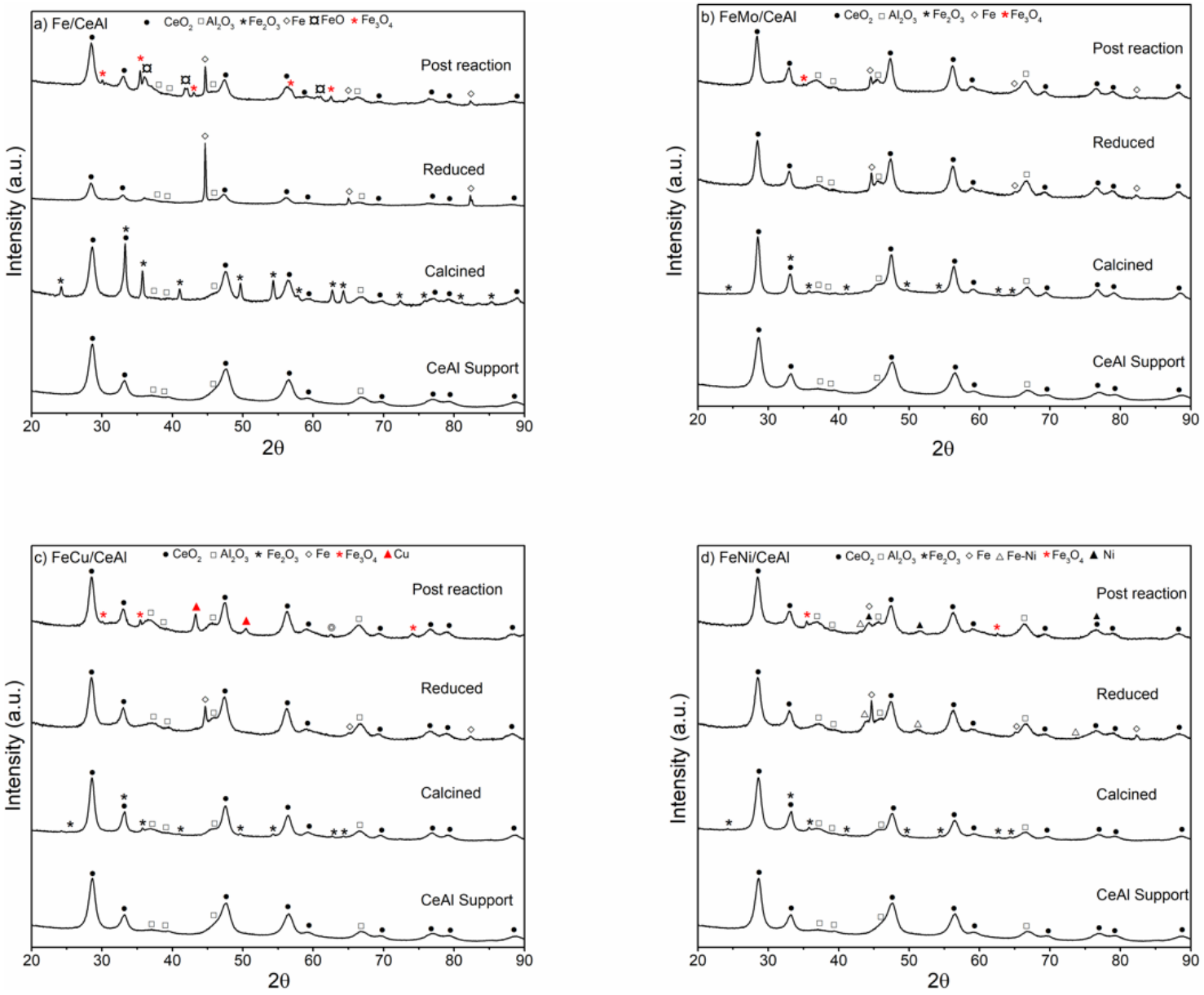

Fig.2 XRD characterisation spectra for all catalyst: (a) Fe/CeAl, (b) FeMo/CeAl, (c) FeCu/CeAl and (d) FeNi/CeAl, calcined, reduced and post reaction, together with the CeAl support.

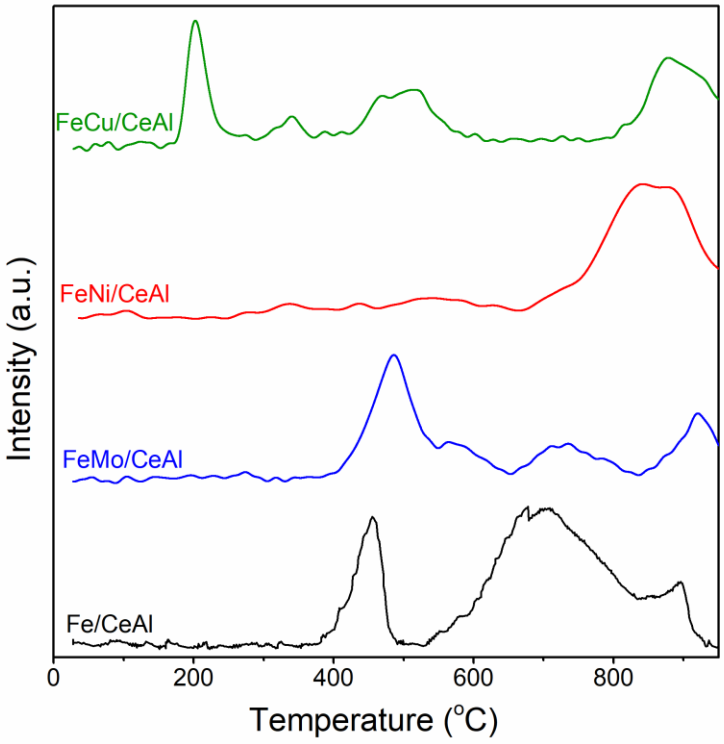

Fig.3 TPR profiles of the calcined samples.

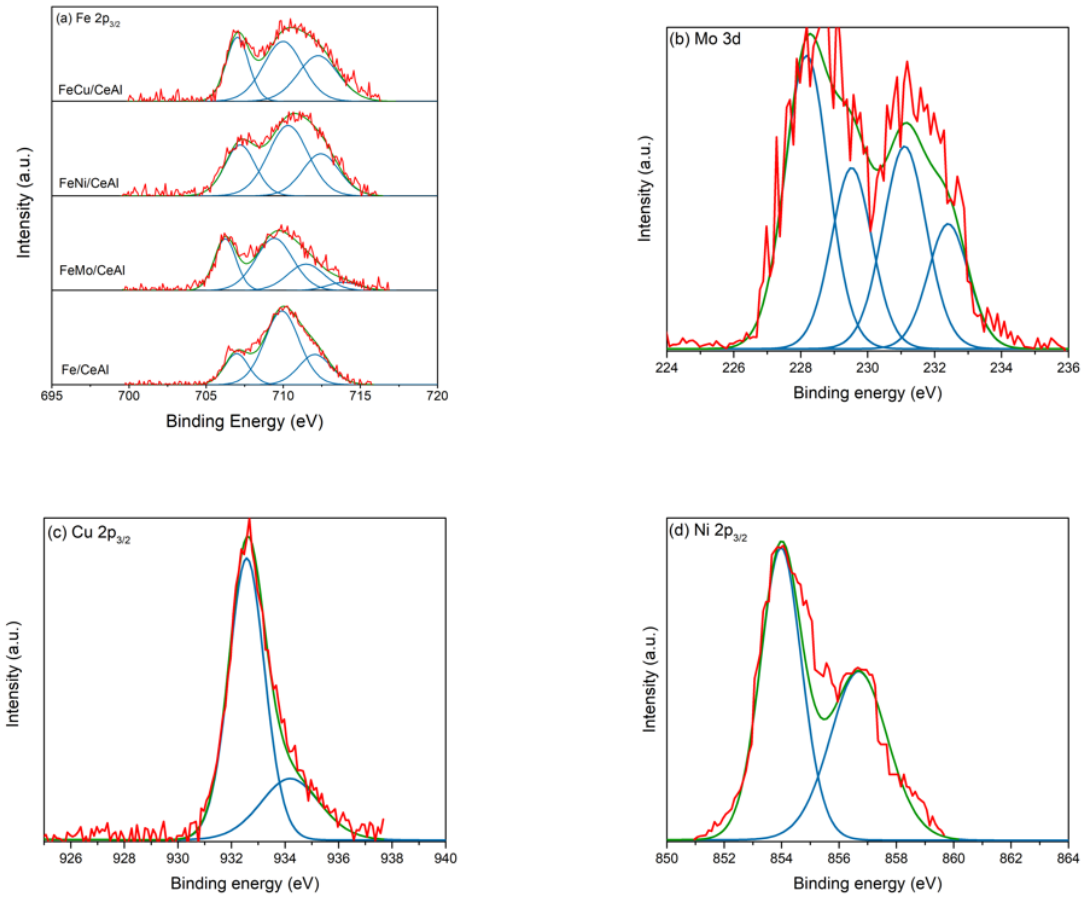

Fig.4 XPS core level of (a) Fe 2p, (b) Mo 3d, (c) Cu 2p and (d) Ni 2p spectra.

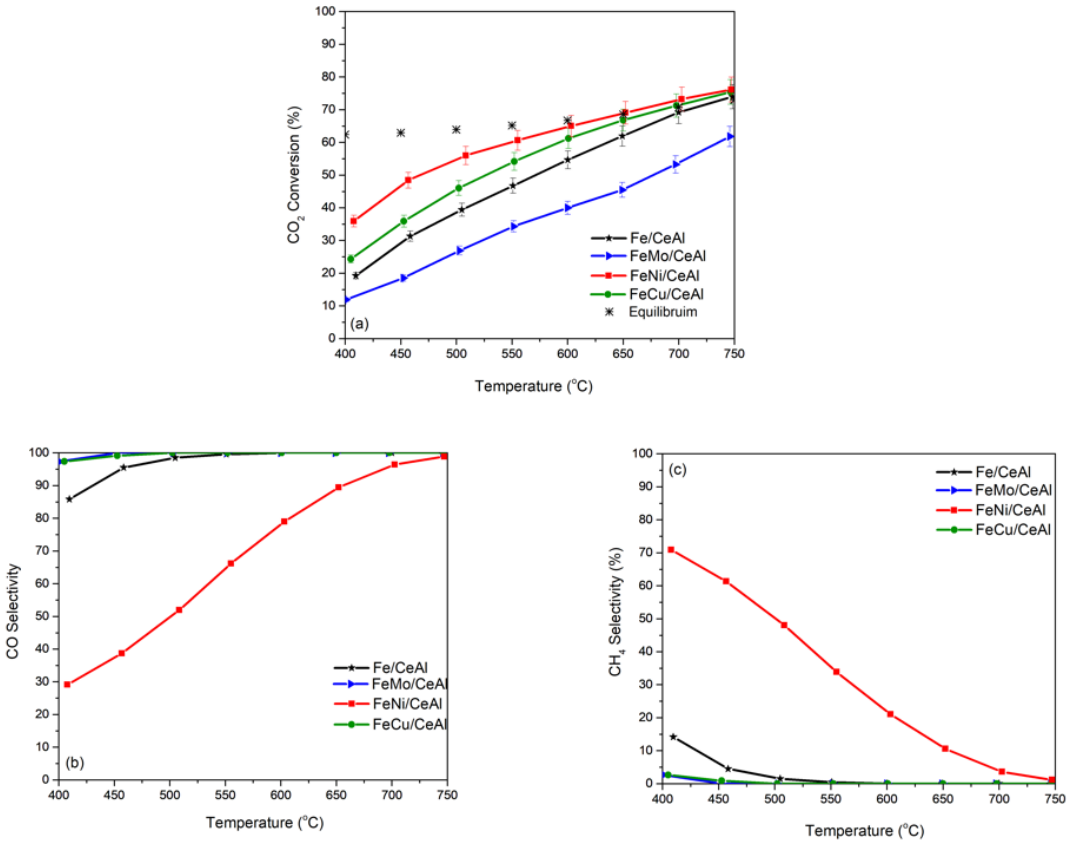

Fig.5 (a) CO_2 conversion, (b) CO selectivity and (c) CH_4 selectivity for all catalysts as a function of temperature.

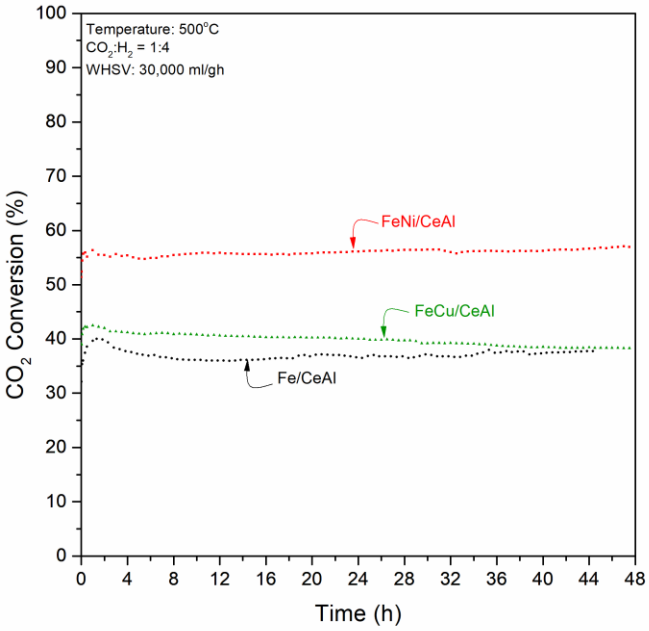

Fig.6 Stability test: CO_2 conversion for Fe/CeAl, FeNi/CeAl and FeCu/CeAl at 500 ^{o}C with a WHSV of 30,000 $mL \cdot g^{-1} \cdot h^{-1}$

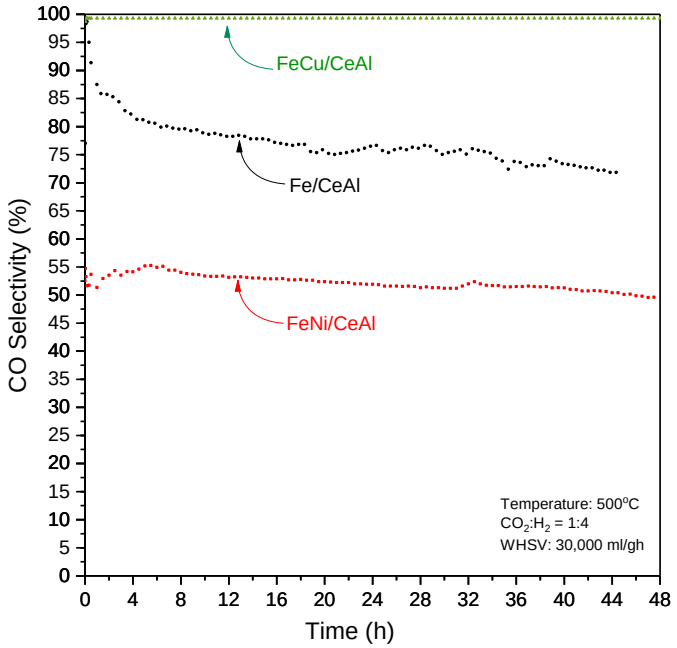

Fig.7 Stability test: CO selectivity for Fe/CeAl, FeNi/CeAl and FeCu/CeAl at 500 ^{o}C with a WHSV of 30,000 mL·g^{-1}·h^{-1}

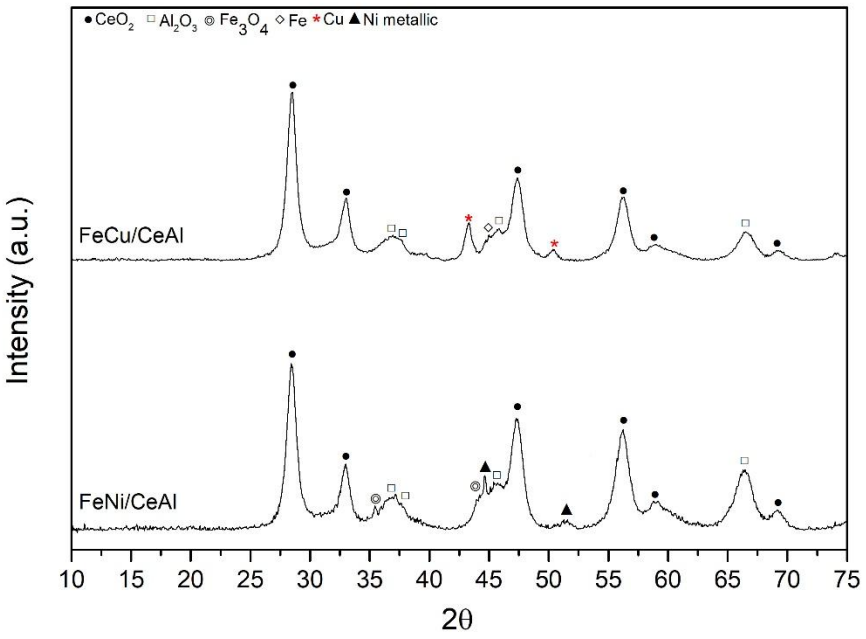

Figure 8. XRD patterns of spent catalysts in long-term tests (500 °C, 30,000 $mL \cdot g^{-1} \cdot h^{-1}$, H_2/CO_2 ratio of 4:1)

Credit Author Statement

L.Yang: Investigation, Writing – Original Draft

L.Pastor-Pérez: Conceptualization, Methodology, Writing – Review & Editing, Supervision, Project administration

J.J.Villora-Pico: Investigation

S.Gu: Funding Acquisition

A.Sepúlveda-Escribano: Writing – Review & Editing, Funding Acquisition

T.R.Reina: Conceptualization, Methodology, Funding Acquisition, Project administration